Multipoint stress mixed finite element methods for elasticity on distorted quadrilateral grids

Ibrahim Yazici* Ivan Yotov*

September 28, 2025

Abstract

We develop multipoint stress mixed finite element methods for linear elasticity with weakly enforced stress symmetry on distorted quadrilateral grids, which can be reduced to positive definite cell-centered systems. The methods utilize the lowest-order Brezzi-Douglas-Marini finite element spaces for the stress and employ vertex quadrature rules to localize the interaction of degrees of freedom. This approach allows for local stress elimination around each vertex. We introduce two methods. The first method uses a piecewise constant rotation, resulting in a cell-centered system for the displacement and the rotation. The second method employs a continuous piecewise bilinear rotation, enabling further elimination of the rotation and resulting in a cell-centered system for the displacement only. The methods utilize a non-symmetric vertex quadrature rule for the stress bilinear form and both non-symmetric and symmetric vertex quadrature rules for the asymmetry bilinear forms. Stability and error analysis are performed for both methods. First-order convergence is established for all variables in the L^2-norm. Numerical results are presented that verify the theoretical results.

1 Introduction

Mixed finite element (MFE) methods for stress-displacement elasticity formulations provide accurate stress representation with local momentum conservation, locking-free approximations, and efficient handling of nearly incompressible materials. Extensive research has examined both strong [10, 15] and weak [11, 13, 14, 16, 17, 21, 25, 27, 30, 35] stress symmetry within these methods. A significant challenge, however, is that they result in algebraic systems saddle point type, which can be computationally expensive to solve. To mitigate this issue, two prevalent approaches are used to convert MFE formulations to positive definite systems: hybridization, which creates skeletal systems, and reduction to cell-centered systems.

In this paper, we develop two stress-displacement MFE methods for elasticity on distorted quadrilateral grids, which can be reduced to positive definite cell-centered systems. These methods, referred to as multipoint stress mixed finite element (MSMFE) methods, are inspired by similar formulations previously developed for simplicial [5], smooth quadrilateral [6], and cuboid [39] grids, as well as the related multipoint stress approximation (MPSA) finite volume method [28, 32]. However, our stability and error analysis on distorted quadrilaterals present significant differences.

The MSMFE approach draws from the multipoint flux mixed finite element (MFMFE) methods [26, 37, 38], which reduce MFE methods for Darcy flow to cell-centered finite differences on various grid types, including simplicial, quadrilateral, and hexahedral. The MFMFE method is closely related to the multipoint flux approximation (MPFA) method [1–4, 22], a finite volume method that eliminates fluxes around mesh vertices in terms of neighboring pressures. This approach accommodates discontinuous full tensor coefficients and general grid structures, offering an improvement over earlier cell-centered finite

*Department of Mathematics, University of Pittsburgh, Pittsburgh, PA 15260, USA; {iby2@pitt.edu, yotov@math.pitt.edu}. Partially supported by NSF grants DMS-2111129 and DMS-2410686.

difference schemes derived from MFE methods, which are effective only for either diagonal tensors and cuboid grids [23, 33] or full tensors with smooth grids and coefficients [7, 8].

The MFMFE methods employ the lowest order Brezzi–Douglas–Marini $\mathcal{BDM}_1$ spaces [19] on simplicial and quadrilateral grids and an enhanced Brezzi–Douglas–Duran–Fortin $\mathcal{BDDF}_1$ space [18] on hexahedral grids. A vertex quadrature rule is used, allowing for local velocity elimination and resulting in a symmetric and positive definite cell-centered system for the pressure. In [37], which inspired this work, a mixed finite element method on general quadrilateral and hexahedral grids is presented. This method reduces to a cell-centered finite difference scheme using a special non-symmetric quadrature rule, see also [29], that yields a positive definite cell-centered system for the pressure by locally eliminating velocities. It is convergent on rough quadrilateral and hexahedral grids, including hexahedra with non-planar faces.

The methods we develop in this paper are related to the non-symmetric MFMFE method [37]. We consider a formulation where the symmetry of the stress is imposed weakly using a Lagrange multiplier, which has a physical interpretation as rotation. We use a non-symmetric vertex quadrature rule for the stress-stress and stress-rotation bilinear forms in the constitutive equation and a symmetric vertex quadrature rule for the stress-rotation bilinear form in the equation for weak imposition of symmetry. The reason for the use of a non-symmetric quadrature rule is that it provides a good approximation on general quadrilaterals, unlike the symmetric quadrature rule, which suffers from reduced accuracy on such grids.

Our first method, referred to as MSMFE-0, is based on the spaces $\mathcal{BDM}_1 \times Q_0 \times Q_0$, employing the $\mathcal{BDM}_1$ space for stress and piecewise constants for the displacement and the rotation. For the $\mathcal{BDM}_1$ space, the degrees of freedom are the values of normal components at any two points on each of the four edges, and we select the vertices for these points. This choice is motivated by the use of the vertex quadrature rule, localizing the interaction of the stress degrees of freedom around the vertices. This results in a block-diagonal stress matrix. The stress is then locally eliminated, reducing the method to a positive definite cell-centered system for the displacement and the rotation, which is smaller and easier to solve than the original system.

Our second method, MSMFE-1, is based on the spaces $\mathcal{BDM}_1 \times Q_0 \times Q_1$, with continuous bilinear rotations. In addition to the initial local stress elimination, since there is one rotation basis function associated with each vertex, we further eliminate the rotation locally. This results in a positive definite cell-centered system for the displacement only.

We perform stability and error analysis for both MSMFE methods. The arguments for distorted quadrilaterals differ from those for smooth quadrilaterals presented in [6] due to the use a non-symmetric vertex quadrature rule for the stress-stress and stress-rotation bilinear forms in the constitutive equation and a symmetric vertex quadrature rule for the weak imposition of symmetry. Employing two different quadrature rules increases the complexity of the analysis and requires a different approach.

We conduct the stability and error analysis for grids with elements that are $h^{1+\alpha}$-perturbations of parallelograms for $\alpha > 0$. In the analysis, we establish a bound for the difference between the stress-rotation bilinear forms with non-symmetric and symmetric quadrature rules. We also utilize the fact that our spaces satisfy an inf-sup condition with symmetric quadrature for the stress-rotation bilinear form, as established in [6] for the MSMFE-1 method. We proceed to establish first-order convergence for the stress, displacement, and rotation in the L^2-norm for both methods. For the quadrature errors, we utilize properties established for the non-symmetric quadrature rule in [37]. We further prove that the resulting algebraic systems for both methods are positive definite and therefore suitable for efficient Krylov space iterative method such as GMRES.

The rest of the paper is organized as follows. Section 2 presents the model problem and its MFE approximation. In Sections 3 and 4 we develop the two methods. The stability and error analyses for both methods are performed in Sections 5 and 6, respectively. Numerical results are presented in Section 7, followed by closing remarks in Section 8.

2 Model problem and its MFE approximation

Let Ω be a simply connected, bounded polygonal domain in $\mathbb{R}^2$. We denote by $\mathbb{M}$, $\mathbb{S}$, and $\mathbb{N}$ the spaces of real 2×2 matrices, symmetric matrices, and skew-symmetric matrices, respectively. We will employ the standard divergence operator div, which, for vector fields, produces a scalar field. When applied to a matrix field, div yields a vector field by taking the divergence of each row of the matrix. Additionally, we use the curl operator, defined as

$$\operatorname{curl} \phi = (\partial_2 \phi, -\partial_1 \phi)$$

for a scalar function ϕ. For a vector field, the curl operator produces a matrix field by applying the operator row-wise.

Throughout the paper, C denotes a generic positive constant that is independent of the discretization parameter h. We will also use the following standard notation. For a domain $G \subset \mathbb{R}^2$, the $L^2(G)$ inner product and norm for scalar and vector-valued functions are denoted by $(\cdot,\cdot)_G$ and $\|\cdot\|_G$, respectively. The norms and seminorms of the Sobolev spaces $W^{k,p}(G)$, $k \in \mathbb{R}, p > 0$ are denoted by $\|\cdot\|_{k,p,G}$ and $|\cdot|_{k,p,G}$, respectively. The norms and seminorms of the Hilbert spaces $H^k(G)$ are denoted by $\|\cdot\|_{k,G}$ and $|\cdot|_{k,G}$, respectively. We omit G in the subscript if $G = \Omega$. For a section of the domain or element boundary S, we write $\langle\cdot,\cdot\rangle_S$ and $\|\cdot\|_S$ for the $L^2(S)$ inner product (or duality pairing) and norm, respectively. We will also use the space $H(\operatorname{div};\Omega) = \{v \in L^2(\Omega,\mathbb{R}^2) : \operatorname{div} v \in L^2(\Omega)\}$ equipped with the norm

$$\|v\|_{\operatorname{div}} = \left(\|v\|^2 + \|\operatorname{div} v\|^2\right)^{1/2}.$$

Given a uniformly positive definite compliance tensor $A \in L^\infty(\Omega,\mathbb{S})$ and a vector field $f \in L^2(\Omega,\mathbb{R}^2)$ representing body forces, the equations of linear elasticity in the Hellinger-Reissner form determine the stress σ and the displacement u satisfying the constitutive and equilibrium equations, respectively:

$$A\sigma = \epsilon(u), \quad \operatorname{div}\sigma = f \quad \text{in } \Omega, \tag{2.1}$$

together with the boundary conditions

$$u = g \ \text{ on } \Gamma_D, \quad \sigma\, n = 0 \ \text{ on } \Gamma_N, \tag{2.2}$$

where $\epsilon(u) = \frac{1}{2}\left(\nabla u + (\nabla u)^T\right)$, $\partial\Omega = \Gamma_D \cup \Gamma_N$, n is the unit outward normal vector on $\partial\Omega$, and $g \in H^{1/2}(\Gamma_D,\mathbb{R}^2)$. We assume that $\Gamma_D \neq \emptyset$, which ensures uniqueness of the solution.

We consider a weak formulation for (2.1)–(2.2), in which the stress symmetry is imposed weakly, using the Lagrange multiplier $\gamma = \operatorname{skew}(\nabla u)$, where $\operatorname{skew}(\tau) = \frac{1}{2}(\tau - \tau^T) \in \mathbb{N}$: find $(\sigma,u,\gamma) \in \mathbb{X} \times V \times \mathbb{W}$ such that

$$(A\sigma,\tau) + (u,\operatorname{div}\tau) + (\gamma,\tau) = \langle g, \tau\, n\rangle_{\Gamma_D}, \qquad \forall \tau \in \mathbb{X}, \tag{2.3}$$

$$(\operatorname{div}\sigma, v) = (f,v), \qquad \forall v \in V, \tag{2.4}$$

$$(\sigma,w) = 0, \qquad \forall w \in \mathbb{W}, \tag{2.5}$$

where the corresponding spaces are

$$\mathbb{X} = \{\tau \in H(\operatorname{div};\Omega,\mathbb{M}) : \tau\, n = 0 \text{ on } \Gamma_N\}, \quad V = L^2(\Omega,\mathbb{R}^2), \quad \mathbb{W} = L^2(\Omega,\mathbb{N}).$$

Problem (2.3)–(2.5) has a unique solution [14].

2.1 Mixed finite element method

Let $\mathcal{T}_h$ be a shape-regular quadrilateral partition of Ω [20], with $h = \max_{E\in\mathcal{T}_h} \operatorname{diam}(E)$. For any element $E \in \mathcal{T}_h$, there exists a bilinear bijection mapping $F_E : \hat{E} \to E$, where $\hat{E} = [0,1]^2$ is the reference square, see Figure 1. Denote the Jacobian matrix by DF_E and let $J_E = |\det(DF_E)|$. For $\mathbf{x} = F_E(\hat{\mathbf{x}})$, we have

$$DF_E^{-1}(\mathbf{x}) = (DF_E)^{-1}(\hat{\mathbf{x}}), \qquad J_{F_E^{-1}}(\mathbf{x}) = \frac{1}{J_E(\hat{\mathbf{x}})}.$$

Let $\hat{E}$ have vertices $\hat{\mathbf{r}}_1 = (0,0)^T$, $\hat{\mathbf{r}}_2 = (1,0)^T$, $\hat{\mathbf{r}}_3 = (1,1)^T$, and $\hat{\mathbf{r}}_4 = (0,1)^T$. We denote by $\mathbf{r}_i = (x_i, y_i)^T$, $i = 1, \ldots, 4$, the corresponding vertices of the element E, The bilinear mapping F_E and its Jacobian matrix are given by

$$F_E(\hat{\mathbf{r}}) = \mathbf{r}_1 + \mathbf{r}_{21}\hat{x} + \mathbf{r}_{41}\hat{y} + (\mathbf{r}_{34} - \mathbf{r}_{21})\hat{x}\hat{y}, \tag{2.6}$$

$$DF_E = [\mathbf{r}_{21}, \mathbf{r}_{41}] + [(\mathbf{r}_{34} - \mathbf{r}_{21})\hat{y}, (\mathbf{r}_{34} - \mathbf{r}_{21})\hat{x}], \tag{2.7}$$

where $\mathbf{r}_{ij} = \mathbf{r}_i - \mathbf{r}_j$.

It is easy to see that the shape-regularity of the grids imply that for all $E \in \mathcal{T}_h$,

$$\|DF_E\|_{0,\infty,\hat{E}} \sim h_E, \quad \|DF_E^{-1}\|_{0,\infty,\hat{E}} \sim h_E^{-1}, \quad \|J_E\|_{0,\infty,\hat{E}} \sim h_E^2, \quad \text{and} \quad \|J_{F_E^{-1}}\|_{0,\infty,\hat{E}} \sim h_E^{-2}, \tag{2.8}$$

where the notation $a \sim b$ means that there exist positive constants c_0, c_1 independent of h such that $c_0 b \le a \le c_1 b$.

The finite element spaces $\mathbb{X}_h \times V_h \times \mathbb{W}_h^k \subset \mathbb{X} \times V \times \mathbb{W}$ are the triple $(\mathcal{BDM}_1)^2 \times (\mathcal{Q}_0)^2 \times (\mathcal{Q}_k)^{2\times 2,\text{skew}}$, $k = 0, 1$, where $\mathcal{Q}_k$ denotes the space of polynomials of degree at most k in each variable and each row of an element of $\mathbb{X}_h$ is a vector in $\mathcal{BDM}_1$. In the case $k = 1$ the rotation space $\mathbb{W}_h^1$ consists of continuous functions. On the reference square the spaces are defined as

$$\begin{aligned}
\hat{\mathbb{X}}(\hat{E}) &= \left(\mathcal{P}_1(\hat{E})^2 + r_1 \operatorname{curl}(\hat{x}^2\hat{y}) + s_1 \operatorname{curl}(\hat{x}\hat{y}^2)\right) \times \left(\mathcal{P}_1(\hat{E})^2 + r_2 \operatorname{curl}(\hat{x}^2\hat{y}) + s_2 \operatorname{curl}(\hat{x}\hat{y}^2)\right) \\
&= \begin{pmatrix} \alpha_1\hat{x} + \beta_1\hat{y} + \gamma_1 + r_1\hat{x}^2 + 2s_1\hat{x}\hat{y} & \alpha_2\hat{x} + \beta_2\hat{y} + \gamma_2 - 2r_1\hat{x}\hat{y} - s_1\hat{y}^2 \\ \alpha_3\hat{x} + \beta_3\hat{y} + \gamma_3 + r_2\hat{x}^2 + 2s_2\hat{x}\hat{y} & \alpha_4\hat{x} + \beta_4\hat{y} + \gamma_4 - 2r_2\hat{x}\hat{y} - s_2\hat{y}^2 \end{pmatrix}, \\
\hat{V}(\hat{E}) &= \left(\mathcal{Q}_0(\hat{E})\right)^2, \quad \hat{\mathbb{W}}^k(\hat{E}) = \begin{pmatrix} 0 & p \\ -p & 0 \end{pmatrix}, \quad p \in \mathcal{Q}_k(\hat{E}) \text{ for } k = 0, 1,
\end{aligned} \tag{2.9}$$

where $\alpha_i, \beta_i, \gamma_i, r_i, s_i$ are real constants. Note that $\operatorname{div} \hat{\mathbb{X}}(\hat{E}) = \hat{V}(\hat{E})$ and for all $\hat{\tau} \in \hat{\mathbb{X}}(\hat{E})$, $\hat{\tau}\,\hat{n}_{\hat{e}} \in \mathcal{P}_1(\hat{e})^2$ on any edge $\hat{e}$ of $\hat{E}$, where $\hat{n}_{\hat{e}}$ is the outward unit normal vector on $\hat{e}$. It is well known [18, 19] that the degrees of freedom of $\mathcal{BDM}_1(\hat{E})$ can be chosen as the values of the normal components at any two points on each edge $\hat{e} \subset \partial\hat{E}$. In this work we choose these points to be the vertices of $\hat{e}$, see Figure 1. This is motivated by the vertex quadrature rules, introduced in the next section. The spaces on any element $E \in \mathcal{T}_h$ are defined via the transformations

$$\tau \overset{\mathcal{P}}{\leftrightarrow} \hat{\tau} : \tau^T = \frac{1}{J_E} DF_E \hat{\tau}^T \circ F_E^{-1}, \quad v \leftrightarrow \hat{v} : v = \hat{v} \circ F_E^{-1}, \quad w \leftrightarrow \hat{w} : \xi = \hat{w} \circ F_E^{-1}, \tag{2.10}$$

where $\hat{\tau} \in \hat{\mathbb{X}}(\hat{E})$, $\hat{v} \in \hat{V}(\hat{E})$, and $\hat{w} \in \hat{\mathbb{W}}^k(\hat{E})$. Note that the Piola transformation (applied row-wise) is used for $\hat{\mathbb{X}}(\hat{E})$. It satisfies, for all sufficiently smooth $\tau \overset{\mathcal{P}}{\leftrightarrow} \hat{\tau}$, $v \leftrightarrow \hat{v}$, and $\phi \leftrightarrow \hat{\phi}$,

$$(\operatorname{div}\tau, v)_E = (\operatorname{div}\hat{\tau}, \hat{v})_{\hat{E}}, \quad \langle \tau\, n_e, v\rangle_e = \langle \hat{\tau}\,\hat{n}_{\hat{e}}, \hat{v}\rangle_{\hat{e}}, \quad \text{and} \quad \operatorname{curl}\phi \overset{\mathcal{P}}{\leftrightarrow} \operatorname{curl}\hat{\phi}. \tag{2.11}$$

The finite element spaces on $\mathcal{T}_h$ are defined by

$$\begin{aligned}
\mathbb{X}_h &= \{\tau \in \mathbb{X} : \tau|_E \overset{\mathcal{P}}{\leftrightarrow} \hat{\tau},\ \hat{\tau} \in \hat{\mathbb{X}}(\hat{E}) \quad \forall E \in \mathcal{T}_h\}, \\
V_h &= \{v \in V : v|_E \leftrightarrow \hat{v},\ \hat{v} \in \hat{V}(\hat{E}) \quad \forall E \in \mathcal{T}_h\}, \\
\mathbb{W}_h^0 &= \{w \in \mathbb{W} : w|_E \leftrightarrow \hat{w},\ \hat{w} \in \hat{\mathbb{W}}^0(\hat{E}) \quad \forall E \in \mathcal{T}_h\}, \\
\mathbb{W}_h^1 &= \{w \in \mathcal{C}(\Omega, \mathbb{N}) \subset \mathbb{W} : w|_E \leftrightarrow \hat{w},\ \hat{w} \in \hat{\mathbb{W}}^1(\hat{E}) \quad \forall E \in \mathcal{T}_h\}.
\end{aligned} \tag{2.12}$$

Note that $\mathbb{W}_h^1 \subset H^1(\Omega)$, since it contains continuous piecewise $\mathcal{Q}_1$ functions.

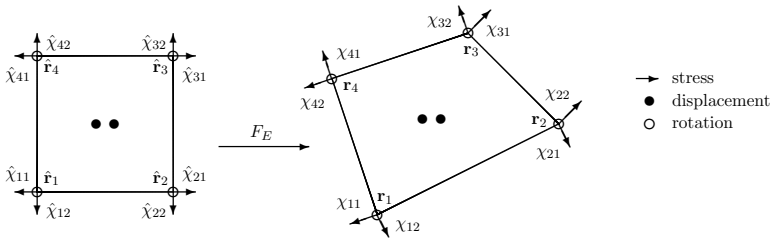

Figure 1: Degrees of freedom of $\mathbb{X}_h \times V_h \times \mathbb{W}_h^1$.

The MFE method for (2.3)–(2.5) is: find $(\sigma_h, u_h, \gamma_h) \in \mathbb{X}_h \times V_h \times \mathbb{W}_h^k$ such that

$$(A\sigma_h, \tau) + (u_h, \operatorname{div} \tau) + (\gamma_h, \tau) = \langle g, \tau n \rangle_{\Gamma_D}, \qquad \tau \in \mathbb{X}_h, \tag{2.13}$$

$$(\operatorname{div} \sigma_h, v) = (f, v), \qquad v \in V_h, \tag{2.14}$$

$$(\sigma_h, w) = 0, \qquad w \in \mathbb{W}_h^k. \tag{2.15}$$

It is shown in [11] that the method (2.13)–(2.15) in the case $k = 0$ has a unique solution and is first-order accurate for all variables in their corresponding norms. The case $k = 1$ on rectangles is analyzed in [30]. The framework from [11] can be used to analyze the case $k = 1$ on quadrilaterals. A drawback of the method is that the resulting algebraic problem is a coupled stress-displacement-rotation system of a saddle point type. In this paper, we develop two methods that utilize symmetric and non-symmetric vertex quadrature rules and can be reduced to cell-centered systems for displacement-rotation and displacement only, respectively.

2.2 Symmetric and non-symmetric quadrature rules

For a continuous function φ on an element $E \in \mathcal{T}_h$, we approximate $\int_E \varphi \, d\mathbf{x}$ by mapping to the reference element and employing the vertex quadrature rule:

$$\int_E \varphi \, d\mathbf{x} = \int_{\hat{E}} \varphi(F_E(\hat{\mathbf{x}})) J_E \, d\hat{\mathbf{x}} \approx \frac{|\hat{E}|}{4} \sum_{i=1}^{4} \varphi(F_E(\hat{\mathbf{r}}_i)) J_E(\hat{\mathbf{r}}_i) = \frac{|\hat{E}|}{4} \sum_{i=1}^{4} \varphi(\mathbf{r}_i) J_E(\hat{\mathbf{r}}_i).$$

Since for τ, $\chi \in \mathbb{X}_h$ we have

$$\int_E A\tau : \chi \, d\mathbf{x} = \int_{\hat{E}} \hat{A} \frac{1}{J_E} \hat{\tau} DF_E^T : \frac{1}{J_E} \hat{\chi} DF_E^T \, J_E \, d\hat{\mathbf{x}} = \int_{\hat{E}} \hat{A}\hat{\tau} \frac{1}{J_E} DF_E^T : \hat{\chi} DF_E^T \, d\hat{\mathbf{x}},$$

the symmetric vertex quadrature rule on an element E is defined as

$$(A\tau, \chi)_{\tilde{Q},E} := \frac{|\hat{E}|}{4} \sum_{i=1}^{4} \hat{A}(\hat{\mathbf{r}}_i) \hat{\tau}(\hat{\mathbf{r}}_i) \frac{1}{J_E(\hat{\mathbf{r}}_i)} DF_E^T(\hat{\mathbf{r}}_i) : \hat{\chi}(\hat{\mathbf{r}}_i) DF_E^T(\hat{\mathbf{r}}_i). \tag{2.16}$$

The non-symmetric vertex quadrature rule [29] on an element E is then defined as

$$(A\tau, \chi)_{Q,E} := \frac{|\hat{E}|}{4} \sum_{i=1}^{4} \overline{A}_E \hat{\tau}(\hat{\mathbf{r}}_i) \frac{1}{J_E(\hat{\mathbf{r}}_i)} DF_E^T(\hat{\mathbf{r}}_i) : \hat{\chi}(\hat{\mathbf{r}}_i) DF_E^T(\hat{\mathbf{r}}_c). \tag{2.17}$$

where $\overline{A}_E$ is the constant tensor with components equal to the mean values of the components of A on E and $\hat{\mathbf{r}}_c$ is the center of mass of $\hat{E}$. The global quadrature rules are defined as

$$(A\tau, \chi)_{\tilde{Q}} := \sum_{E \in \mathcal{T}_h} (A\tau, \chi)_{\tilde{Q},E} \quad \text{and} \quad (A\tau, \chi)_Q := \sum_{E \in \mathcal{T}_h} (A\tau, \chi)_{Q,E}.$$

We also employ the vertex quadrature rules for the stress-rotation bilinear forms. Since for $\tau \in \mathbb{X}_h$, $w \in \mathbb{W}_h^k$ we have

$$\int_E \tau : w \, d\mathbf{x} = \int_{\hat{E}} \frac{1}{J_E} \hat{\tau} DF_E^T : \hat{w} J_E \, d\hat{\mathbf{x}} = \int_{\hat{E}} \hat{\tau} DF_E^T : \hat{w} \, d\hat{\mathbf{x}},$$

we define

$$(\tau, w)_{\tilde{Q},E} = (w, \tau)_{\tilde{Q},E} := \frac{|\hat{E}|}{4} \sum_{i=1}^{4} \hat{\tau}(\hat{\mathbf{r}}_i) DF_E^T(\hat{\mathbf{r}}_i) : \hat{w}(\hat{\mathbf{r}}_i), \tag{2.18}$$

$$(\tau, w)_{Q,E} = (w, \tau)_{Q,E} := \frac{|\hat{E}|}{4} \sum_{i=1}^{4} \hat{\tau}(\hat{\mathbf{r}}_i) DF_E^T(\hat{\mathbf{r}}_c) : \hat{w}(\hat{\mathbf{r}}_i), \tag{2.19}$$

with

$$(\tau, w)_{\tilde{Q}} := \sum_{E \in \mathcal{T}_h} (\tau, w)_{\tilde{Q},E} \quad \text{and} \quad (\tau, w)_Q := \sum_{E \in \mathcal{T}_h} (\tau, w)_{Q,E}.$$

The following lemma and assumption establish that the vertex quadrature rules generate coercive bilinear forms.

Lemma 2.1. [6] *The bilinear form $(A\tau, \chi)_{\tilde{Q}}$ is an inner product on $\mathbb{X}_h$ and $(A\tau, \tau)_{\tilde{Q}}^{1/2}$ is a norm in $\mathbb{X}_h$ equivalent to $\|\cdot\|$, that is, there exist constants $0 < \tilde{\alpha}_0 \leq \tilde{\alpha}_1$ independent of h such that*

$$\tilde{\alpha}_0 \|\tau\|^2 \leq (A\tau, \tau)_{\tilde{Q}} \leq \tilde{\alpha}_1 \|\tau\|^2 \quad \forall \tau \in \mathbb{X}_h. \tag{2.20}$$

Furthermore, $(w, w)_{\tilde{Q}}^{1/2}$ is a norm in $\mathbb{W}_h^k$ equivalent to $\|\cdot\|$, and $\forall\, \tau \in \mathbb{X}_h$, $w \in \mathbb{W}_h^k$, $(\tau, w)_{\tilde{Q}} \leq C\|\tau\|\|w\|$.

Assumption 2.1. *$(A\tau, \tau)_Q^{1/2}$ is a norm in $\mathbb{X}_h$ equivalent to $\|\cdot\|$, that is, there exist constants $0 < \alpha_0 \leq \alpha_1$ independent of h such that*

$$\alpha_0 \|\tau\|^2 \leq (A\tau, \tau)_Q \leq \alpha_1 \|\tau\|^2 \quad \forall \tau \in \mathbb{X}_h. \tag{2.21}$$

In addition, it holds that

$$(A\tau, \chi)_Q \leq C\|\tau\|\|\chi\| \quad \forall \tau, \chi \in \mathbb{X}_h,$$

and $\forall \tau \in \mathbb{X}_h$, $w \in \mathbb{W}_h^k$, it holds that $(\tau, w)_Q \leq C\|\tau\|\|w\|$.

It is shown in [37, Lemma 3.13] that Assumption 2.1 holds under certain conditions on the shape regularity of the elements and the anisotropy of compliance tensor A, see also [29, 31] for further details on these conditions.

For the analysis of the methods, we impose a restriction on the element geometry. A quadrilateral with vertices $\mathbf{r}_1, \ldots, \mathbf{r}_4$ is called an $h^{1+\alpha}$ parallelogram if

$$|\mathbf{r}_{34} - \mathbf{r}_{21}|_{\mathbb{R}^2} \leq C h_E^{1+\alpha}, \tag{2.22}$$

where $|\cdot|_{\mathbb{R}^2}$ is the Euclidean vector norm. It is not difficult to check that in this case

$$|DF_E|_{1,\infty,\hat{E}} \leq C h_E^{1+\alpha}. \tag{2.23}$$

We have the following bound on the stress-rotation bilinear forms with the symmetric and non-symmetric quadrature rules given in (2.18) and (2.19).

Lemma 2.2. *For a mesh of $h^{1+\alpha}$ parallelograms, there exists a constant $\tilde{C} > 0$ independent of h such that*

$$|(\tau, w)_Q - (\tau, w)_{\tilde{Q}}| \leq \tilde{C} h^{\alpha} \|\tau\|\|w\|. \tag{2.24}$$

Proof. Using the definitions of the quadrature rules (2.18) and (2.19), we have the following on each element E:

$$\begin{aligned}
|(\tau,w)_{Q,E}-(\tau,w)_{\tilde{Q},E}| &= \frac{|\hat{E}|}{4}\left|\sum_{i=1}^{4}\hat{\tau}(\hat{\mathbf{r}}_i)DF_E^T(\hat{\mathbf{r}}_c):\hat{w}(\hat{\mathbf{r}}_i)-\sum_{i=1}^{4}\hat{\tau}(\hat{\mathbf{r}}_i)DF_E^T(\hat{\mathbf{r}}_i):\hat{w}(\hat{\mathbf{r}}_i)\right| \\
&= \frac{|\hat{E}|}{4}\left|\sum_{i=1}^{4}\hat{\tau}(\hat{\mathbf{r}}_i)\left(DF_E^T(\hat{\mathbf{r}}_c)-DF_E^T(\hat{\mathbf{r}}_i)\right):\hat{w}(\hat{\mathbf{r}}_i)\right| \\
&= \frac{|\hat{E}|}{4}\left|\sum_{i=1}^{4}\hat{\tau}(\hat{\mathbf{r}}_i)\frac{1}{J_E(\hat{\mathbf{r}}_i)}DF_E^T(\hat{\mathbf{r}}_i)DF_E^{-T}(\hat{\mathbf{r}}_i)\left(DF_E^T(\hat{\mathbf{r}}_c)-DF_E^T(\hat{\mathbf{r}}_i)\right):\hat{w}(\hat{\mathbf{r}}_i)J_E(\hat{\mathbf{r}}_i)\right| \\
&\le C\|DF_E^{-1}\|_{0,\infty,\hat{E}}\,|DF_E|_{1,\infty,\hat{E}}\,\|\tau\circ F_E\|_{\hat{E}}\|w\circ F_E\|_{\hat{E}}\|J_E\|_{0,\infty,\hat{E}} \\
&\le Ch_E^{-1}h_E^{1+\alpha}\|\tau\|_E\|w\|_E\|J_{F_E^{-1}}\|_{0,\infty,\hat{E}}\|J_E\|_{0,\infty,\hat{E}} \\
&= Ch_E^{\alpha}\|\tau\|_E\|w\|_E, \qquad (2.25)
\end{aligned}$$

where we have used (2.8) and (2.23). The proof is completed by summing over E. □

3 The multipoint stress mixed finite element method with constant rotations (MSMFE-0)

Let $\mathcal{P}_0$ be the L^2-orthogonal projection onto the space of piecewise constant vector-valued functions on the trace of $\mathcal{T}_h$ on $\partial\Omega$. Our first method, referred to as MSMFE-0, is: find $\sigma_h\in\mathbb{X}_h$, $u_h\in V_h$, and $\gamma_h\in\mathbb{W}_h^0$ such that

$$\begin{aligned}
(A\sigma_h,\tau)_Q+(u_h,\operatorname{div}\tau)+(\gamma_h,\tau)_Q &= \langle\mathcal{P}_0 g,\tau\,n\rangle_{\Gamma_D}, && \tau\in\mathbb{X}_h, && (3.1)\\
(\operatorname{div}\sigma_h,v) &= (f,v), && v\in V_h, && (3.2)\\
(\sigma_h,w)_{\tilde{Q}} &= 0, && w\in\mathbb{W}_h^0. && (3.3)
\end{aligned}$$

The Dirichlet data is incorporated into the scheme as $\mathcal{P}_0 g$, which is necessary for the optimal approximation of the boundary data term.

Remark 3.1. *Note that the non-symmetric quadrature rule $(\cdot,\cdot)_Q$ is employed in the constitutive equation* (3.1)*, which is needed for the consistency of the method, while the symmetric quadrature rule $(\cdot,\cdot)_{\tilde{Q}}$ is employed in* (3.3)*. The latter is motivated by the fact that the definition of the symmetric quadrature rule* (2.18) *implies that for $\sigma\in\mathbb{S}$ and $\xi\in\mathbb{N}$,*

$$(\sigma,\xi)_{\tilde{Q}}=0, \qquad (3.4)$$

while (3.4) *does not hold with the non-symmetric quadrature rule $(\sigma,\xi)_Q$ defined in* (2.19)*.*

The following assumption is required for the analysis of the MSMFE-0 method. It is proved for a special case in Appendix A.

Assumption 3.1. *There exists a constant $\beta_1>0$ independent of h such that*

$$\inf_{0\neq(v,w)\in V_h\times\mathbb{W}_h^0}\sup_{0\neq\tau\in\mathbb{X}_h}\frac{(\operatorname{div}\tau,v)+(\tau,w)_{\tilde{Q}}}{\|\tau\|_{\operatorname{div}}\left(\|v\|+\|w\|\right)}\ge\beta_1. \qquad (3.5)$$

Remark 3.2. *The above inf-sup condition without quadrature rule, i.e. with $(\tau,w)_{\tilde{Q}}$ replaced by (τ,w), is established in [11]. The argument used there cannot be extended to the case with quadrature rule.*

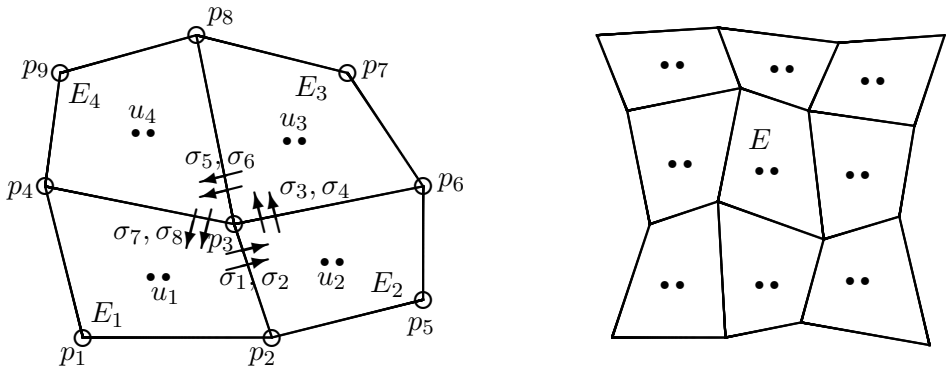

Figure 2: Finite elements sharing a vertex (left) and displacement stencil (right)

3.1 Reduction to a cell-centered displacement-rotation system

The algebraic system resulting from (3.1)–(3.3) takes the form

$$\begin{pmatrix} A_{\sigma\sigma} & A_{\sigma u}^T & A_{\sigma\gamma}^T \\ -A_{\sigma u} & 0 & 0 \\ -\tilde{A}_{\sigma\gamma} & 0 & 0 \end{pmatrix} \begin{pmatrix} \sigma \\ u \\ \gamma \end{pmatrix} = \begin{pmatrix} g \\ -f \\ 0 \end{pmatrix}, \tag{3.6}$$

where $(A_{\sigma\sigma})_{ij} = (A\tau_j, \tau_i)_Q$, $(A_{\sigma u})_{ij} = (\operatorname{div} \tau_j, v_i)$, $(A_{\sigma\gamma})_{ij} = (\tau_j, w_i)_Q$, and $(\tilde{A}_{\sigma\gamma})_{ij} = (\tau_j, w_i)_{\tilde{Q}}$. This system can be reduced to a cell-centered displacement-rotation form as follows.

Since the quadrature rule $(A\sigma_h, \tau)_Q$ confines basis function interactions to mesh vertices, the matrix $A_{\sigma\sigma}$ becomes block-diagonal, with $2k \times 2k$ blocks corresponding to vertices, where k is the number of elements sharing the vertex. Figure 2 (left) illustrates an example with $k = 4$. Due to Assumption 2.1 these blocks are positive definite, allowing the stress variable σ_h to be efficiently eliminated by solving small local systems. This reduction yields the cell-centered displacement-rotation system

$$\begin{pmatrix} A_{\sigma u} A_{\sigma\sigma}^{-1} A_{\sigma u}^T & A_{\sigma u} A_{\sigma\sigma}^{-1} A_{\sigma\gamma}^T \\ \tilde{A}_{\sigma\gamma} A_{\sigma\sigma}^{-1} A_{\sigma u}^T & \tilde{A}_{\sigma\gamma} A_{\sigma\sigma}^{-1} A_{\sigma\gamma}^T \end{pmatrix} \begin{pmatrix} u \\ \gamma \end{pmatrix} = \begin{pmatrix} -f + A_{\sigma u} A_{\sigma\sigma}^{-1} g \\ \tilde{A}_{\sigma\gamma} A_{\sigma\sigma}^{-1} g \end{pmatrix}. \tag{3.7}$$

The displacement and rotation stencils for an element E involve all elements sharing a vertex with E, as shown in Figure 2 (right) for a sample displacement stencil.

Lemma 3.1. *Assuming that h is sufficiently small, the system in* (3.7) *is positive definite.*

Proof. We aim to show that, for any $\begin{pmatrix} v^T & w^T \end{pmatrix} \neq 0$,

$$\begin{pmatrix} v^T & w^T \end{pmatrix} \begin{pmatrix} A_{\sigma u} A_{\sigma\sigma}^{-1} A_{\sigma u}^T & A_{\sigma u} A_{\sigma\sigma}^{-1} A_{\sigma\gamma}^T \\ \tilde{A}_{\sigma\gamma} A_{\sigma\sigma}^{-1} A_{\sigma u}^T & \tilde{A}_{\sigma\gamma} A_{\sigma\sigma}^{-1} A_{\sigma\gamma}^T \end{pmatrix} \begin{pmatrix} v \\ w \end{pmatrix} > 0. \tag{3.8}$$

Let τ, v, w be vectors corresponding to the stress, displacement, and rotation finite element functions τ_h, v_h, w_h. Define the scaled vectors $\tilde{v}$ and $\tilde{w}$ such that $\tilde{v}|_E = h_E\, v|_E$ and $\tilde{w}|_E = h_E\, w|_E$. Due to (2.10) and (2.8) we have

$$|\tau|_{\mathbb{R}^2} \sim \|\tau_h\|, \quad |\tilde{v}|_{\mathbb{R}^2} \sim \|v_h\|, \quad |\tilde{w}|_{\mathbb{R}^2} \sim \|w_h\|. \tag{3.9}$$

We write

$$
\begin{aligned}
|A_{\sigma u}^T v + A_{\sigma\gamma}^T w|_{\mathbb{R}^2} &= \sup_{\tau} \frac{\left(A_{\sigma u}^T v + A_{\sigma\gamma}^T w\right)\cdot \tau}{|\tau|} \geq C \sup_{\tau_h \in \mathbb{X}_h} \frac{(\operatorname{div} \tau_h, v_h) + (\tau_h, w_h)_Q}{\|\tau_h\|} \\
&= C \sup_{\tau_h \in \mathbb{X}_h} \frac{(\operatorname{div} \tau_h, v_h) + (\tau_h, w_h)_Q - (\tau_h, w_h)_{\tilde{Q}} + (\tau_h, w_h)_{\tilde{Q}}}{\|\tau_h\|} \\
&\geq C \left(\sup_{\tau_h \in \mathbb{X}_h} \frac{(\operatorname{div} \tau_h, v_h) + (\tau_h, w_h)_{\tilde{Q}}}{\|\tau_h\|_{\operatorname{div}}} - \tilde{C} h^{\alpha} \|w_h\| \right) \\
&\geq C \left(\|v_h\| + \|w_h\| - \tilde{C} h^{\alpha} \|w_h\| \right) \\
&\geq C \left(\|v_h\| + \|w_h\| \right) \geq C \left(|\tilde{v}|_{\mathbb{R}^2} + |\tilde{w}|_{\mathbb{R}^2} \right), \qquad (3.10)
\end{aligned}
$$

where we used (3.9) in the first inequality, (2.24) in the second inequality, (3.5) in the third inequality and (3.9) in the last inequality. The fourth inequality above is obtained for h small enough. We also have

$$
|(A_{\sigma\gamma}^T - \tilde{A}_{\sigma\gamma}^T) w|_{\mathbb{R}^2} = \sup_{\tau} \frac{(A_{\sigma\gamma}^T - \tilde{A}_{\sigma\gamma}^T) w \cdot \tau}{|\tau|_{\mathbb{R}^2}} \leq C \sup_{\tau_h \in \mathbb{X}_h} \frac{(\tau_h, w_h)_Q - (\tau_h, w_h)_{\tilde{Q}}}{\|\tau_h\|} \leq C h^{\alpha} \|w_h\| \leq C h^{\alpha} |\tilde{w}|_{\mathbb{R}^2}, \qquad (3.11)
$$

where we used (3.9) in the first and last inequalities, and (2.24) in the second inequality.

Now, for any $\begin{pmatrix} v^T & w^T \end{pmatrix} \neq 0$, we write

$$
\begin{aligned}
&\begin{pmatrix} v^T & w^T \end{pmatrix} \begin{pmatrix} A_{\sigma u} A_{\sigma\sigma}^{-1} A_{\sigma u}^T & A_{\sigma u} A_{\sigma\sigma}^{-1} A_{\sigma\gamma}^T \\ \tilde{A}_{\sigma\gamma} A_{\sigma\sigma}^{-1} A_{\sigma u}^T & \tilde{A}_{\sigma\gamma} A_{\sigma\sigma}^{-1} A_{\sigma\gamma}^T \end{pmatrix} \begin{pmatrix} v \\ w \end{pmatrix} \\
&\quad = \left(A_{\sigma u} A_{\sigma\sigma}^{-1} A_{\sigma u}^T v, v\right) + \left(A_{\sigma u} A_{\sigma\sigma}^{-1} A_{\sigma\gamma}^T w, v\right) + \left(\tilde{A}_{\sigma\gamma} A_{\sigma\sigma}^{-1} A_{\sigma u}^T v, w\right) + \left(\tilde{A}_{\sigma\gamma} A_{\sigma\sigma}^{-1} A_{\sigma\gamma}^T w, w\right) \\
&\quad = \left(A_{\sigma\sigma}^{-1} (A_{\sigma u}^T v + A_{\sigma\gamma}^T w), (A_{\sigma u}^T v + \tilde{A}_{\sigma\gamma}^T w)\right) \\
&\quad = \left(A_{\sigma\sigma}^{-1} (A_{\sigma u}^T v + A_{\sigma\gamma}^T w), (A_{\sigma u}^T v + A_{\sigma\gamma}^T w) + (\tilde{A}_{\sigma\gamma}^T - A_{\sigma\gamma}^T) w\right) \\
&\quad \geq C |A_{\sigma u}^T v + A_{\sigma\gamma}^T w|_{\mathbb{R}^2}^2 - C |A_{\sigma u}^T v + A_{\sigma\gamma}^T w|_{\mathbb{R}^2} \, |(\tilde{A}_{\sigma\gamma}^T - A_{\sigma\gamma}^T) w|_{\mathbb{R}^2} \\
&\quad \geq C |A_{\sigma u}^T v + A_{\sigma\gamma}^T w|_{\mathbb{R}^2}^2 - \varepsilon |A_{\sigma u}^T v + A_{\sigma\gamma}^T w|_{\mathbb{R}^2}^2 - C_{\varepsilon} |(\tilde{A}_{\sigma\gamma}^T - A_{\sigma\gamma}^T) w|_{\mathbb{R}^2}^2 \\
&\quad \geq C |A_{\sigma u}^T v + A_{\sigma\gamma}^T w|_{\mathbb{R}^2}^2 - C |(\tilde{A}_{\sigma\gamma}^T - A_{\sigma\gamma}^T) w|_{\mathbb{R}^2}^2 \\
&\quad \geq C \left(|\tilde{v}|_{\mathbb{R}^2}^2 + |\tilde{w}|_{\mathbb{R}^2}^2\right) - C h^{2\alpha} |\tilde{w}|_{\mathbb{R}^2}^2 \geq C \left(|\tilde{v}|_{\mathbb{R}^2}^2 + |\tilde{w}|_{\mathbb{R}^2}^2\right) > 0, \qquad (3.12)
\end{aligned}
$$

where we used (2.21) in the first inequality, Young's inequality in the second inequality, and (3.10) and (3.11) in the fourth inequality. We also used that h is small enough in the last inequality. □

Remark 3.3. *The MSMFE-0 method offers greater efficiency than the original MFE method by solving a smaller, positive definite system. To illustrate the computational savings, consider a logically rectangular grid where the number of elements and vertices are approximately equal, denoted by m. In the original system* (3.6)*, each vertex has eight stress degrees of freedom, while each element has two displacement and one rotation degrees of freedom, totaling around $11m$ unknowns. The reduced system* (3.7)*, however, has only about $3m$ unknowns, resulting in a substantial reduction. Furthermore, the reduced system is positive definite, allowing for efficient solvers such as GMRES to be employed. In contrast, the original system* (3.6) *is indefinite, making such fast solvers unsuitable.*

It is also worth noting that the additional cost for solving local vertex systems, necessary to assemble (3.7)*, is $O(m)$, which becomes negligible for large m in comparison to the $O(m^2)$ cost of solving the global systems* (3.6) *or* (3.7) *with a Krylov space iterative method.*

No further reduction of the system in (3.7) *is possible. In the following section, we introduce a method that uses continuous bilinear rotations with vertex quadrature rules applied to the stress-rotation bilinear forms. This approach allows for further local elimination of the rotation variable, resulting in a cell-centered system for the displacement only.*

4 The multipoint stress mixed finite element method with bilinear rotations (MSMFE-1)

In the second method, called MSMFE-1, we set $k = 1$ in (2.9). The method is: find $\sigma_h \in \mathbb{X}_h$, $u_h \in V_h$, and $\gamma_h \in \mathbb{W}_h^1$ such that

$$(A\sigma_h, \tau)_Q + (u_h, \operatorname{div} \tau) + (\gamma_h, \tau)_Q = \langle \mathcal{P}_0 g, \tau\, n\rangle_{\Gamma_D}, \qquad \tau \in \mathbb{X}_h, \tag{4.1}$$

$$(\operatorname{div} \sigma_h, v) = (f, v), \qquad v \in V_h, \tag{4.2}$$

$$(\sigma_h, w)_{\tilde{Q}} = 0, \qquad w \in \mathbb{W}_h^1. \tag{4.3}$$

We make the following assumptions on the mesh.

Assumption 4.1. *Each element E has at most one edge on Γ_N.*

Assumption 4.2. *The mesh size h is sufficiently small and there exists a constant C such that for every pair of neighboring elements E and $\widetilde{E}$ such that E or $\widetilde{E}$ is a non-parallelogram, and every pair of edges $e \subset \partial E \setminus \partial \widetilde{E}$, $\widetilde{e} \subset \partial \widetilde{E} \setminus \partial E$ that share a vertex,*

$$|\mathbf{r}_e - \mathbf{r}_{\widetilde{e}}|^2_{\mathbb{R}^2} \leq Ch^2,$$

where $\mathbf{r}_e$ and $\mathbf{r}_{\widetilde{e}}$ are the vectors corresponding to e and $\widetilde{e}$, respectively.

The following theorem is proved in [6].

Theorem 4.1. *Under Assumptions* (4.1) *and* (4.2)*, there exists a constant $\beta_2 > 0$ independent of h such that*

$$\inf_{0\neq(v,w)\in V_h\times\mathbb{W}_h^1} \sup_{0\neq\tau\in\mathbb{X}_h} \frac{(\operatorname{div}\tau, v) + (\tau, w)_{\tilde{Q}}}{\|\tau\|_{\operatorname{div}} (\|v\| + \|w\|)} \geq \beta_2. \tag{4.4}$$

4.1 Reduction to a cell-centered displacement system of the MSMFE-1 method

The algebraic system resulting from (4.1)–(4.3) takes the form of (3.6). Similar to the MSMFE-0 method, the quadrature rule in $(A\sigma_h, \tau)_Q$ in (4.1) restricts basis function interactions to vertices, making the matrix $A_{\sigma\sigma}$ block-diagonal with $2k \times 2k$ blocks, where k represents the number of elements sharing a vertex. This structure allows for the elimination of the stress variable, reducing the system to the displacement-rotation form (3.7). The matrix in (3.7) is positive definite, which follows from the proof of Lemma 3.1 by replacing $\tilde{w}|_E = h_E\, w|_E$ with $\tilde{w}|_{\mathbf{r}} = \left(\frac{1}{s}\sum_{i=1}^{s} h_{E_i}\right) w|_{\mathbf{r}}$ where E_i, $i = 1, \ldots, s$, are the elements that share the vertex $\mathbf{r}$, and using the inf-sup condition (4.4).

Additionally, the quadrature rules in the stress-rotation bilinear forms $(\gamma_h, \tau)_Q$ and $(\sigma_h, w)_{\tilde{Q}}$ also localize interactions to vertices, since each vertex has an associated rotation basis function. Consequently, the matrices $A_{\sigma\gamma}$ and $\tilde{A}_{\sigma\gamma}$ are block-diagonal with $1 \times 2k$ blocks, leading to a diagonal rotation matrix $\tilde{A}_{\sigma\gamma} A_{\sigma\sigma}^{-1} A_{\sigma\gamma}^T$. Thus, the rotation variable γ_h can be readily eliminated from (3.7), resulting in the cell-centered displacement system

$$\left(A_{\sigma u} A_{\sigma\sigma}^{-1} A_{\sigma u}^T - A_{\sigma u} A_{\sigma\sigma}^{-1} A_{\sigma\gamma}^T (\tilde{A}_{\sigma\gamma} A_{\sigma\sigma}^{-1} A_{\sigma\gamma}^T)^{-1} \tilde{A}_{\sigma\gamma} A_{\sigma\sigma}^{-1} A_{\sigma u}^T\right) u = \hat{f}. \tag{4.5}$$

We will now establish the positive definiteness of this system by presenting the following lemma.

Lemma 4.1. *Let* $M = \begin{pmatrix} A & B \\ C & D \end{pmatrix}$ *be a block matrix, where* D *is invertible. If* M *is positive definite, then the Schur complement of* D *in* M*, defined by* $A - BD^{-1}C$*, is also positive definite.*

Proof. For any $v \neq 0$, we have

$$\left(\left(A - BD^{-1}C\right)v, v\right) = \left(M \begin{pmatrix} v \\ -D^{-1}Cv \end{pmatrix}, \begin{pmatrix} v \\ -D^{-1}Cv \end{pmatrix}\right) > 0,$$

where the inequality follows from the positive definiteness of M. This completes the proof. □

Corollary 4.1. *The system in* (4.5) *is positive definite.*

Proof. Since the system in (4.5) is the Schur complement of $\tilde{A}_{\sigma\gamma}A_{\sigma\sigma}^{-1}A_{\sigma\gamma}^T$ in the positive definite system (3.7), Lemma 4.1 implies that the system in (4.5) is also positive definite. □

Remark 4.1. *The MSMFE-1 method is more efficient than both the MSMFE-0 and the original MFE methods, as it results in a smaller algebraic system. For example, on a logically rectangular grid with approximately* m *elements and vertices, the MSMFE-1 system* (4.5) *has around* $2m$ *unknowns, compared to* $3m$ *in the MSMFE-0 system* (3.7) *and* $11m$ *in the MFE system* (3.6)*.*

5 Stability analysis of the methods

We establish the solvability of the proposed methods.

Lemma 5.1. *Under Assumptions 2.1, 3.1, 4.1, and 4.2, if* h *is sufficiently small, the MSMFE-0 method* (3.1)–(3.3) *and the MSMFE-1 method* (4.1)–(4.3) *each has a unique solution.*

Proof. We will provide the proof for the MSMFE-1 method; the proof for the MSMFE-0 method follows similarly. Since (4.1)–(4.3) forms a square system, it suffices to demonstrate uniqueness. Let $f = 0$, $g = 0$, and set $\tau = \sigma_h$, $v = u_h$, and $w = \gamma_h$. From the system (4.1)–(4.3), we obtain

$$(A\sigma_h, \sigma_h)_Q + (\sigma_h, \gamma_h)_Q - (\sigma_h, \gamma_h)_{\tilde{Q}} = 0. \tag{5.1}$$

Applying (2.21) and (2.24) to (5.1) gives

$$\alpha_0\|\sigma_h\|^2 \leq \tilde{C}h^\alpha\|\sigma_h\|\|\gamma_h\| \leq \frac{\tilde{C}^2h^{2\alpha}}{2\varepsilon}\|\sigma_h\|^2 + \frac{\varepsilon}{2}\|\gamma_h\|^2, \quad \varepsilon > 0. \tag{5.2}$$

Using the inf-sup condition (4.4) for the symmetric quadrature and (4.1), we get

$$\|u_h\| + \|\gamma_h\| \leq \beta_2^{-1} \sup_{0\neq\tau\in\mathbb{X}_h} \frac{-(A\sigma_h, \tau)_Q + (\tau, \gamma_h)_{\tilde{Q}} - (\tau, \gamma_h)_Q}{\|\tau\|_{\mathrm{div}}} \leq C\left(\|\sigma_h\| + \tilde{C}h^\alpha\|\gamma_h\|\right), \tag{5.3}$$

where we used (2.21) and (2.24). Taking h small enough so that $C\tilde{C}h^\alpha \leq \frac{1}{2}$, we obtain

$$\|u_h\|^2 + \|\gamma_h\|^2 \leq C_1\|\sigma_h\|^2. \tag{5.4}$$

Using (5.4) in (5.2) gives

$$\alpha_0\|\sigma_h\|^2 \leq \frac{\tilde{C}^2h^{2\alpha}}{2\varepsilon}\|\sigma_h\|^2 + \frac{\varepsilon}{2}C_1\|\sigma_h\|^2. \tag{5.5}$$

Choosing $\varepsilon = \varepsilon_0$ small enough in (5.5) such that $\alpha_0 - \frac{\varepsilon_0}{2}C_1 = \frac{1}{2}$, we obtain

$$\|\sigma_h\|^2 \leq \frac{\tilde{C}^2h^{2\alpha}}{\varepsilon_0}\|\sigma_h\|^2. \tag{5.6}$$

Assuming that h is small enough such that $\frac{\tilde{C}^2h^{2\alpha}}{\varepsilon_0} \leq \frac{1}{2}$ in (5.6), we conclude that $\sigma_h = 0$. Finally, by (5.4), we find $u_h = \gamma_h = 0$, completing the proof. □

6 Error Estimates

In this section we establish convergence for all variables. We will first provide several results concerning general quadrilateral elements that will be used in analysis.

6.1 Preliminaries

In the analysis, we will use several projection operators. It is known [18] that there exists an interpolant $\Pi : \mathbb{X} \cap H^1(\Omega, \mathbb{M}) \to \mathbb{X}_h$ such that

$$(\mathrm{div}(\Pi\tau - \tau), v) = 0, \quad \forall v \in V_h. \tag{6.1}$$

The operator Π is defined locally on each element E by $\Pi\tau \overset{\mathcal{P}}{\leftrightarrow} \hat{\Pi}\hat{\tau}$, where $\hat{\Pi}$ is an interpolant on the reference element. We will also use a similar interpolant in the lowest order Raviart-Thomas space:

$$\hat{\mathbb{X}}^{\mathcal{RT}}(\hat{E}) = \begin{pmatrix} \alpha_1 + \beta_1\hat{x} \\ \alpha_2 + \beta_2\hat{y} \end{pmatrix} \times \begin{pmatrix} \alpha_3 + \beta_3\hat{x} \\ \alpha_4 + \beta_4\hat{y} \end{pmatrix}.$$

The degrees of freedom of $\hat{\mathbb{X}}^{\mathcal{RT}}(\hat{E})$ are defined by the values of the normal components at the midpoints of the edges. An interpolant $\Pi^{\mathcal{RT}}$ in $\mathbb{X}_h^{\mathcal{RT}}$, similar to Π above, exists [18] and satisfies, for any edge e,

$$\langle (\Pi^{\mathcal{RT}}\tau - \tau)n_e, \chi n_e\rangle_e = 0, \quad \forall \chi \in \mathbb{X}_h^{\mathcal{RT}}. \tag{6.2}$$

It follows that $\Pi^{\mathcal{RT}}$ satisfies

$$\mathrm{div}\ \tau = \mathrm{div}\ \Pi^{\mathcal{RT}}\tau, \quad \forall \tau \in \mathbb{X}_h, \tag{6.3}$$

and

$$\|\Pi^{\mathcal{RT}}\tau\| \le \|\tau\|, \quad \forall \tau \in \mathbb{X}_h. \tag{6.4}$$

Since the normal trace space $\mathbb{X}_h^{\mathcal{RT}}n$ consists of piecewise constant vector-valued functions on the trace of T_h along $\partial\Omega$, the L^2-projection operator $\mathcal{P}_0$ used in (3.1) can be equivalently characterized as,

$$\text{for any } \phi \in L^2(\partial\Omega, \mathbb{R}^2), \quad \mathcal{P}_0\phi \in \mathbb{X}_h^{\mathcal{RT}}n \text{ such that } \langle \phi - \mathcal{P}_0\phi, \tau n\rangle_{\partial\Omega} = 0, \quad \forall \tau \in \mathbb{X}_h^{\mathcal{RT}}. \tag{6.5}$$

Let Q_h^u be a projection operator onto V_h such that, for any $v \in L^2(\Omega, \mathbb{R}^2)$,

$$\langle \hat{Q}^u\hat{v} - \hat{v}, \hat{w}\rangle_{\hat{E}} = 0, \quad \forall \hat{w} \in \hat{V}(\hat{E}), \quad Q_h^u v = \hat{Q}^u\hat{v} \circ F_E^{-1} \quad \forall E \in T_h.$$

From (2.11), it follows that

$$(Q_h^u v - v, \mathrm{div}\,\tau) = 0, \quad \forall \tau \in \mathbb{X}_h. \tag{6.6}$$

Let $Q_h^{\gamma_k}$ be the L^2-orthogonal projection operator onto $\mathbb{W}_h^k$ such that, for any $w \in L^2(\Omega, \mathbb{N})$,

$$(Q_h^{\gamma_k}w - w, \eta) = 0, \quad \forall \eta \in \mathbb{W}_h^k.$$

Also, let $Q_h^{\sigma_k}$, $k = 0, 1$, be the L^2-orthogonal projection onto the spaces of symmetric piecewise constant and bilinear tensors $Q_k(\Omega, \mathbb{S})$, satisfying, for any $\tau \in L^2(\Omega, \mathbb{S})$,

$$(Q_h^{\sigma_k}\tau - \tau, \chi) = 0, \quad \forall \chi \in Q_k(\Omega, \mathbb{S}).$$

The following lemma states the well-known approximation properties of the operators defined above.

Lemma 6.1. *The following bounds hold:*

$$\|v - Q_h^u v\| \le C\|v\|_r h^r \qquad \forall v \in H^r(\Omega, \mathbb{R}^2), \qquad 0 \le r \le 1, \tag{6.7}$$

$$\|w - Q_h^{\gamma_k}w\| \le C\|w\|_r h^r \qquad \forall w \in H^r(\Omega, \mathbb{N}), \qquad 0 \le r \le 1, \tag{6.8}$$

$$\|\tau - Q_h^{\sigma_k}\tau\| \le C\|\tau\|_r h^r \qquad \forall \tau \in H^r(\Omega, \mathbb{S}), \qquad 0 \le r \le 1, \tag{6.9}$$

$$\|\tau - \Pi\tau\| \le C\|\tau\|_1 h \qquad \forall \tau \in H^1(\Omega, \mathbb{M}), \tag{6.10}$$

$$\|\tau - \Pi^{\mathcal{RT}}\tau\| \le C\|\tau\|_1 h \qquad \forall \tau \in H^1(\Omega, \mathbb{M}). \tag{6.11}$$

Proof. Bound (6.7) follows from a scaling argument and the application of the Bramble-Hilbert lemma [20] on $\hat{E}$. Bounds (6.8) and (6.9) are derived by applying the Bramble-Hilbert lemma on E, noting that $\mathbb{W}_h^k$ includes constant functions on E. Bound (6.10) and (6.11) can be found in [12,36]. □

The following properties of the quadrature rule will be used in the error analysis.

Lemma 6.2. [37, Lemma 2.2] *For any constant tensor σ_0 on E and $\chi \in \mathbb{X}_h(E)$,*

$$(A\sigma_0, \chi - \Pi^{\mathcal{RT}}\chi)_{Q,E} = 0. \tag{6.12}$$

Lemma 6.3. [37, Lemma 2.4] *For any constant tensor σ_0 on E and $\mu \in \mathbb{X}_h^{\mathcal{RT}}(E)$,*

$$(A\sigma_0, \mu)_{Q,E} = (\overline{A}_E\sigma_0, \mu)_E. \tag{6.13}$$

Additionally, we have

$$\|A - \overline{A}_E\|_E \le Ch\|A\|_{1,\infty,E}. \tag{6.14}$$

We denote $A \in W^{1,\infty}_{\mathcal{T}_h}$ if $A \in W^{1,\infty}(E)$ for all $E \in \mathcal{T}_h$, and $\|A\|_{1,\infty,E}$ is uniformly bounded independently of h.

6.2 Convergence analysis

We are now ready to present the convergence analysis for the MSMFE-0 and MSMFE-1 methods.

Theorem 6.1. *Let $A \in W^{1,\infty}_{\mathcal{T}_h}$. If the solution (σ, u, γ) of (2.3)–(2.5) is sufficiently smooth, then, if h is sufficiently small, for the numerical solution $(\sigma_h, u_h, \gamma_h)$ obtained using either the MSMFE-0 method (3.1)–(3.3) or the MSMFE-1 method (4.1)–(4.3), there exists a constant $C > 0$ independent of h such that*

$$\|\sigma - \sigma_h\| + \|u - u_h\| + \|\gamma - \gamma_h\| \le Ch(\|\sigma\|_1 + \|u\|_1 + \|\gamma\|_1). \tag{6.15}$$

Proof. We present the argument for the MSMFE-1 method; the analysis for the MSMFE-0 method is similar. We form the error system by subtracting the MSMFE-1 method (4.1)–(4.2) from (2.3)–(2.4):

$$(A\sigma, \tau) - (A\sigma_h, \tau)_Q + (u - u_h, \operatorname{div}\tau) + (\gamma, \tau) - (\gamma_h, \tau)_Q = \langle g - \mathcal{P}_0 g, \tau\, n\rangle_{\Gamma_D}, \qquad \tau \in \mathbb{X}_h, \tag{6.16}$$

$$(\operatorname{div}(\sigma - \sigma_h), v) = 0, \qquad v \in V_h, \tag{6.17}$$

Using (6.6), (6.2), and (6.5), we rewrite the first error equation as

$$\begin{aligned}(A(\Pi\sigma - \sigma_h), \tau)_Q + (Q_h^u u - u_h, \operatorname{div}\tau)& \\ = -(A\sigma, \tau) + (A\Pi\sigma, \tau)_Q - (\gamma, \tau) + (\gamma_h, \tau)_Q + \langle g, (\tau - \Pi^{\mathcal{RT}}\tau)\, n\rangle_{\Gamma_D}.&\end{aligned} \tag{6.18}$$

For the first two terms on the right above we write

$$\begin{aligned}-(A\sigma, \tau) + (A\Pi\sigma, \tau)_Q = &-(A\sigma, \tau - \Pi^{\mathcal{RT}}\tau) - (A(\sigma - \Pi\sigma), \Pi^{\mathcal{RT}}\tau) \\ &-(A\Pi\sigma, \Pi^{\mathcal{RT}}\tau) + (A\Pi\sigma, \Pi^{\mathcal{RT}}\tau)_Q + (A\Pi\sigma, \tau - \Pi^{\mathcal{RT}}\tau)_Q.\end{aligned} \tag{6.19}$$

The second two terms on the right in (6.18) can be written as

$$\begin{aligned}-(\gamma, \tau) + (\gamma_h, \tau)_Q =& -(\gamma, \tau - \Pi^{\mathcal{RT}}\tau) - (\gamma - Q_h^{\gamma_0}\gamma, \Pi^{\mathcal{RT}}\tau) \\ &- (Q_h^{\gamma_0}\gamma, \Pi^{\mathcal{RT}}\tau) + (Q_h^{\gamma_0}\gamma, \Pi^{\mathcal{RT}}\tau)_Q \\ &+ (Q_h^{\gamma_0}\gamma, \tau - \Pi^{\mathcal{RT}}\tau)_Q + (\gamma_h - Q_h^{\gamma_1}\gamma, \tau)_Q + (Q_h^{\gamma_1}\gamma - Q_h^{\gamma_0}\gamma, \tau)_Q \\ =& -(\gamma, \tau - \Pi^{\mathcal{RT}}\tau) - (\gamma - Q_h^{\gamma_0}\gamma, \Pi^{\mathcal{RT}}\tau) \\ &+ (\gamma_h - Q_h^{\gamma_1}\gamma, \tau)_Q + (Q_h^{\gamma_1}\gamma - Q_h^{\gamma_0}\gamma, \tau)_Q,\end{aligned} \tag{6.20}$$

using (6.13) with $A = I$ for the third and forth terms and (6.12) with $A = I$ for the fifth term on the right-hand side of the first equation. We now combine (6.18)–(6.20). Noting that the combination of the first terms on the right-hand sides of (6.19) and (6.20) with the last term in (6.18) gives

$$-(A\sigma, \tau - \Pi^{\mathcal{RT}}\tau) - (\gamma, \tau - \Pi^{\mathcal{RT}}\tau) + \langle g, (\tau - \Pi^{\mathcal{RT}}\tau)\, n\rangle_{\Gamma_D} = 0, \tag{6.21}$$

which follows from testing (2.3) with $\tau - \Pi^{\mathcal{RT}}\tau$ and using (6.3), we obtain

$$\begin{aligned}
&(A(\Pi\sigma - \sigma_h), \tau)_Q + (Q_h^u u - u_h, \operatorname{div}\tau) \\
&\quad = -(A(\sigma - \Pi\sigma), \Pi^{\mathcal{RT}}\tau) - (A\Pi\sigma, \Pi^{\mathcal{RT}}\tau) + (A\Pi\sigma, \Pi^{\mathcal{RT}}\tau)_Q + (A\Pi\sigma, \tau - \Pi^{\mathcal{RT}}\tau)_Q \\
&\qquad - (\gamma - Q_h^{\gamma_0}\gamma, \Pi^{\mathcal{RT}}\tau) + (\gamma_h - Q_h^{\gamma_1}\gamma, \tau)_Q + (Q_h^{\gamma_1}\gamma_h - Q_h^{\gamma_0}\gamma, \tau)_Q.
\end{aligned} \tag{6.22}$$

The terms on the right hand side of (6.22) are bounded as follows. Using (6.10) and (6.4), we have

$$|(A(\sigma - \Pi\sigma), \Pi^{\mathcal{RT}}\tau)| \le Ch\|\sigma\|_1\|\tau\| \le Ch^2\|\sigma\|_1^2 + \varepsilon\|\tau\|^2. \tag{6.23}$$

Next, using (6.13), we know that

$$(AQ_h^{\sigma_0}\sigma, \Pi^{\mathcal{RT}}\tau)_Q = (\overline{A}Q_h^{\sigma_0}\sigma, \Pi^{\mathcal{RT}}\tau).$$

Using the above, the second and third terms on the right in (6.22) can be bounded as

$$\begin{aligned}
&-(A\Pi\sigma, \Pi^{\mathcal{RT}}\tau) + (A\Pi\sigma, \Pi^{\mathcal{RT}}\tau)_Q = (\overline{A}Q_h^{\sigma_0}\sigma - A\Pi\sigma, \Pi^{\mathcal{RT}}\tau) + (A(\Pi\sigma - Q_h^{\sigma_0}\sigma), \Pi^{\mathcal{RT}}\tau)_Q \\
&\quad = ((\overline{A} - A)Q_h^{\sigma_0}\sigma, \Pi^{\mathcal{RT}}\tau) + (A(Q_h^{\sigma_0}\sigma - \sigma), \Pi^{\mathcal{RT}}\tau) + (A(\sigma - \Pi\sigma), \Pi^{\mathcal{RT}}\tau) + (A(\Pi\sigma - Q_h^{\sigma_0}\sigma), \Pi^{\mathcal{RT}}\tau)_Q \\
&\quad \le Ch\|\sigma\|_1\|\tau\| \le Ch^2\|\sigma\|_1^2 + \varepsilon\|\tau\|^2,
\end{aligned} \tag{6.24}$$

using (6.14), (6.4), (6.9), (6.10), and Lemma 2.1. For the fourth term on the right in (6.22), using (6.12), (6.4), (6.9), (6.10), and Lemma 2.1 we write

$$(A\Pi\sigma, \tau - \Pi^{\mathcal{RT}}\tau)_Q = (A(\Pi\sigma - Q_h^{\sigma_0}\sigma), \tau - \Pi^{\mathcal{RT}}\tau)_Q \le Ch\|\sigma\|_1\|\tau\| \le Ch^2\|\sigma\|_1^2 + \varepsilon\|\tau\|^2. \tag{6.25}$$

For the fifth term on the right in (6.22), using (6.8) and (6.4), we have

$$-(\gamma - Q_h^{\gamma_0}\gamma, \Pi^{\mathcal{RT}}\tau) \le Ch\|\gamma\|_1\|\tau\| \le Ch^2\|\gamma\|_1^2 + \varepsilon\|\tau\|^2. \tag{6.26}$$

For the last term on the right in (6.22), using (6.8), we get

$$(Q_h^{\gamma_1}\gamma - Q_h^{\gamma_0}\gamma, \tau)_Q \le Ch^2\|\gamma\|_1^2 + \varepsilon\|\tau\|^2. \tag{6.27}$$

Combining (6.22)–(6.27), we obtain

$$(A(\Pi\sigma - \sigma_h), \tau)_Q + (Q_h^u u - u_h, \operatorname{div}\tau) \le Ch^2(\|\sigma\|_1^2 + \|\gamma\|_1^2) + \varepsilon\|\tau\|^2 + (\gamma_h - Q_h^{\gamma_1}\gamma, \tau)_Q. \tag{6.28}$$

We next note that, using (6.1), the second error equation (6.17) implies that

$$\operatorname{div}(\Pi\sigma - \sigma_h) = 0. \tag{6.29}$$

We set $\tau = \Pi\sigma - \sigma_h$ in (6.28) and take ε small enough to obtain

$$\|\Pi\sigma - \sigma_h\|^2 \le Ch^2(\|\sigma\|_1^2 + \|\gamma\|_1^2) + (\gamma_h - Q_h^{\gamma_1}\gamma, \Pi\sigma - \sigma_h)_Q. \tag{6.30}$$

For the last term in (6.30) we can write

$$\begin{aligned}
(\gamma_h - Q_h^{\gamma_1}\gamma, \Pi\sigma - \sigma_h)_Q =& (\gamma_h - Q_h^{\gamma_1}\gamma, \Pi\sigma - \sigma_h)_Q - (\gamma_h - Q_h^{\gamma_1}\gamma, \Pi\sigma - \sigma_h)_{\tilde{Q}} \\
&+ (\gamma_h - Q_h^{\gamma_1}\gamma, \Pi\sigma - \sigma_h)_{\tilde{Q}}.
\end{aligned} \tag{6.31}$$

Using (2.24) for the first two terms on the right in (6.31), we get

$$(\gamma_h - Q_h^{\gamma_1}\gamma, \Pi\sigma - \sigma_h)_Q - (\gamma_h - Q_h^{\gamma_1}\gamma, \Pi\sigma - \sigma_h)_{\tilde{Q}} \leq \tilde{C}h^{\alpha}\|\Pi\sigma - \sigma_h\|\|\gamma_h - Q_h^{\gamma_1}\gamma\| \\ \leq Ch^{2\alpha}\|\Pi\sigma - \sigma_h\|^2 + \varepsilon\|\gamma_h - Q_h^{\gamma_1}\gamma\|^2. \tag{6.32}$$

For the last term in (6.31) we have

$$(\gamma_h - Q_h^{\gamma_1}\gamma, \Pi\sigma - \sigma_h)_{\tilde{Q}} = (\gamma_h - Q_h^{\gamma_1}\gamma, \Pi\sigma)_{\tilde{Q}} = (\gamma_h - Q_h^{\gamma_1}\gamma, \Pi\sigma - Q_h^{\sigma_1}\sigma)_{\tilde{Q}} \\ \leq Ch\|\sigma\|_1\|\gamma_h - Q_h^{\gamma_1}\gamma\| \leq Ch^2\|\sigma\|_1^2 + \varepsilon\|\gamma_h - Q_h^{\gamma_1}\gamma\|^2, \tag{6.33}$$

using (4.3), (3.4), Lemma 2.1, (6.9), and (6.10). Combining (6.30)–(6.33), and taking h small enough, we obtain

$$\|\Pi\sigma - \sigma_h\|^2 \leq Ch^2(\|\sigma\|_1^2 + \|\gamma\|_1^2) + \varepsilon\|\gamma_h - Q_h^{\gamma_1}\gamma\|^2. \tag{6.34}$$

Now, we apply the inf-sup condition (4.4) to $(Q_h^u u - u_h, Q_h^{\gamma_1}\gamma - \gamma_h) \in V_h \times \mathbb{W}_h^1$ and use (6.16) to obtain

$$\|Q_h^u u - u_h\| + \|Q_h^{\gamma_1}\gamma - \gamma_h\| \\ \leq C \sup_{\tau \in \mathbb{X}_h} \frac{-(A\sigma, \tau) + (A\sigma_h, \tau)_Q - (\gamma, \tau) + (\gamma_h, \tau)_Q + (Q_h^{\gamma_1}\gamma - \gamma_h, \tau)_{\tilde{Q}} + \langle g - \mathcal{P}_0 g, \tau\, n\rangle_{\Gamma_D}}{\|\tau\|_{\mathrm{div}}}. \tag{6.35}$$

The numerator can be rewritten as

$$-(A\sigma, \tau) + (A\sigma_h, \tau)_Q - (\gamma, \tau) + (Q_h^{\gamma_1}\gamma, \tau)_Q + \langle g, (\tau - \Pi^{\mathcal{RT}}\tau)\, n\rangle_{\Gamma_D} + (Q_h^{\gamma_1}\gamma - \gamma_h, \tau)_{\tilde{Q}} - (Q_h^{\gamma_1}\gamma - \gamma_h, \tau)_Q. \tag{6.36}$$

We rewrite the first two terms in (6.36) similarly to (6.18)–(6.19):

$$-(A\sigma, \tau) + (A\sigma_h, \tau)_Q = -(A(\Pi\sigma - \sigma_h), \tau)_Q - (A\sigma, \tau - \Pi^{\mathcal{RT}}\tau) - (A(\sigma - \Pi\sigma), \Pi^{\mathcal{RT}}\tau) \\ - (A\Pi\sigma, \Pi^{\mathcal{RT}}\tau) + (A\Pi\sigma, \Pi^{\mathcal{RT}}\tau)_Q + (A\Pi\sigma, \tau - \Pi^{\mathcal{RT}}\tau)_Q. \tag{6.37}$$

In a way similar to (6.20), we rewrite the second two terms in (6.36) as

$$-(\gamma, \tau) + (Q_h^{\gamma_1}\gamma, \tau)_Q = -(\gamma, \tau - \Pi^{\mathcal{RT}}\tau) - (\gamma - Q_h^{\gamma_0}\gamma, \Pi^{\mathcal{RT}}\tau) + (Q_h^{\gamma_1}\gamma - Q_h^{\gamma_0}\gamma, \tau)_Q. \tag{6.38}$$

Using (6.37), (6.38), and (6.21), for terms in (6.36) we obtain

$$-(A(\Pi\sigma - \sigma_h), \tau)_Q - (A(\sigma - \Pi\sigma), \Pi^{\mathcal{RT}}\tau) - (A\Pi\sigma, \Pi^{\mathcal{RT}}\tau) + (A\Pi\sigma, \Pi^{\mathcal{RT}}\tau)_Q + (A\Pi\sigma, \tau - \Pi^{\mathcal{RT}}\tau)_Q \\ - (\gamma - Q_h^{\gamma_0}\gamma, \Pi^{\mathcal{RT}}\tau) + (Q_h^{\gamma_1}\gamma - Q_h^{\gamma_0}\gamma, \tau)_Q + (Q_h^{\gamma_1}\gamma - \gamma_h, \tau)_{\tilde{Q}} - (Q_h^{\gamma_1}\gamma - \gamma_h, \tau)_Q. \tag{6.39}$$

Using bounds (6.23)–(6.25) for the second to fifth terms in (6.39), (6.26)–(6.27) for the sixth and seven terms, and (2.24) for the last two terms, (6.35) implies

$$\|Q_h^u u - u_h\| + \|Q_h^{\gamma_1}\gamma - \gamma_h\| \leq C(h\|\sigma\|_1 + h\|\gamma\|_1 + h^{\alpha}\|Q_h^{\gamma_1}\gamma - \gamma_h\| + \|\Pi\sigma - \sigma_h\|). \tag{6.40}$$

Next, we combine a sufficiently small multiple of (6.40) with (6.34), and choose ε in (6.34) small enough, obtaining

$$\|\Pi\sigma - \sigma_h\| + \|Q_h^u u - u_h\| + \|Q_h^{\gamma_1}\gamma - \gamma_h\| \leq Ch(\|\sigma\|_1 + \|\gamma\|_1). \tag{6.41}$$

The assertion of the theorem follows from (6.41) and the approximation bounds (6.7)–(6.10). □

7 Numerical Results

In this section we present numerical experiments to corroborate the theoretical findings discussed in the earlier sections. We evaluate the convergence of the MSMFE-0 and MSMFE-1 methods across various quadrilateral grid types. The implementation is carried out using the deal.II finite element library [9].

We consider a homogeneous and isotropic medium characterized by

$$A\sigma = \frac{1}{2\mu}\left(\sigma - \frac{\lambda}{2\mu + 2\lambda}\mathrm{tr}(\sigma)I\right), \tag{7.1}$$

where I denotes the 2×2 identity matrix, and $\mu > 0$, $\lambda > -\mu$ represent the Lamé coefficients. For the domain $\Omega = (0,1)^2$, we address the elasticity problem as formulated in (2.1) and (2.2), incorporating Dirichlet boundary conditions. The exact solution is expressed as

$$u_0 = \begin{pmatrix} \cos(\pi x)\sin(2\pi y) \\ \cos(\pi y)\sin(\pi x) \end{pmatrix}, \tag{7.2}$$

with the Lamé coefficients set as $\lambda = 123$ and $\mu = 79.3$.

In the first three examples we test square, h^2-parallelogram, and smooth quadrilateral meshes, for which the symmetric MSMFE methods developed in [6] provide first-order convergence. The square grids in the first test are created through sequential uniform refinement of an initial mesh with a characteristic size of $h = 1/2$. In the second test, we start with a general quadrilateral grid. A sequence of finer meshes is then generated by dividing each element into four equal parts in successive steps. This approach yields h^2-parallelogram grids. For the third test, a sequence of smooth quadrilateral meshes is considered. Each mesh is crafted by applying a smooth transformation $\mathbf{x} = \hat{\mathbf{x}} + 0.1\sin(2\pi\hat{x})\sin(2\pi\hat{y})\begin{pmatrix}1\\1\end{pmatrix}$ to a uniformly refined square mesh, starting from $h = 1/2$.

Tables 1–6 present the convergence results on these grids for the MSMFE-0 and MSMFE-1 methods. Additionally, Figures 3–5 display the computed solutions on these meshes for the MSMFE-1 method. We observe at least first-order convergence in the L^2-norm for all variables and the divergence of the stress. The latter is expected on smooth grids, due to (6.29) and the $\mathcal{O}(h)$ approximation for $\|\operatorname{div}(\sigma - \Pi\sigma)\|$ [18]. In addition, we observe that the $\mathcal{O}(h^2)$ superconvergence for $\|Q_h^u u - u_h\|$ in the symmetric methods shown in [6, Theorem 5.2] carries over to the non-symmetric methods.

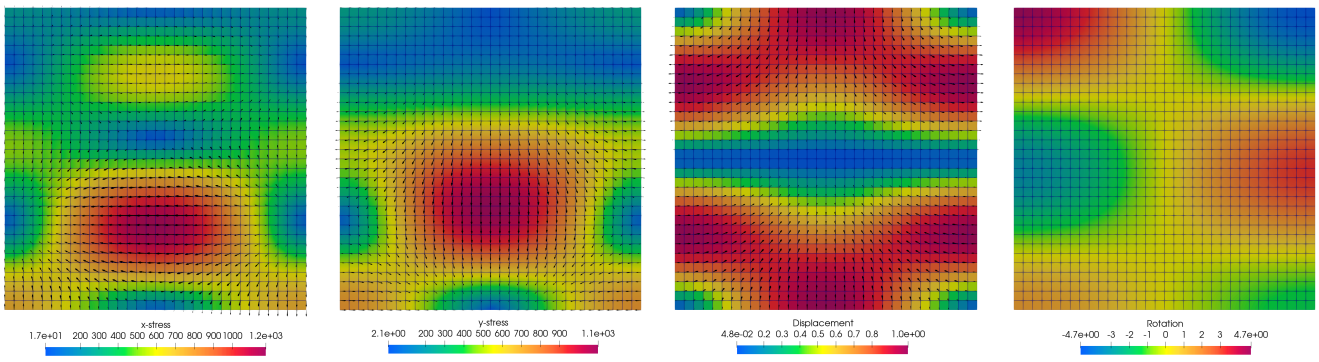

(a) x-stress (b) y-stress (c) Displacement (d) Rotation

Figure 3: Computed solution on a square mesh via the MSMFE-1 method, $h = 1/32$.

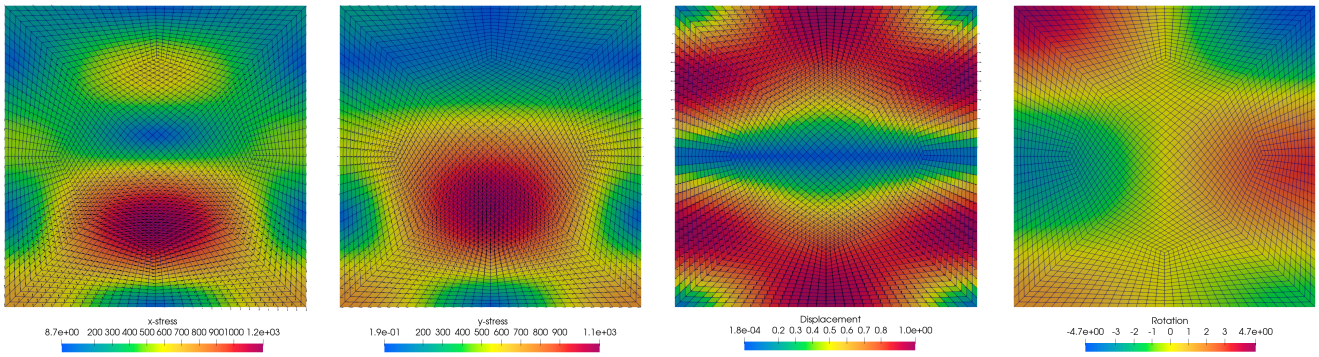

(a) x-stress (b) y-stress (c) Displacement (d) Rotation

Figure 4: Computed solution on a h^2-parallelogram mesh via the MSMFE-1 method, $h = 1/48$.

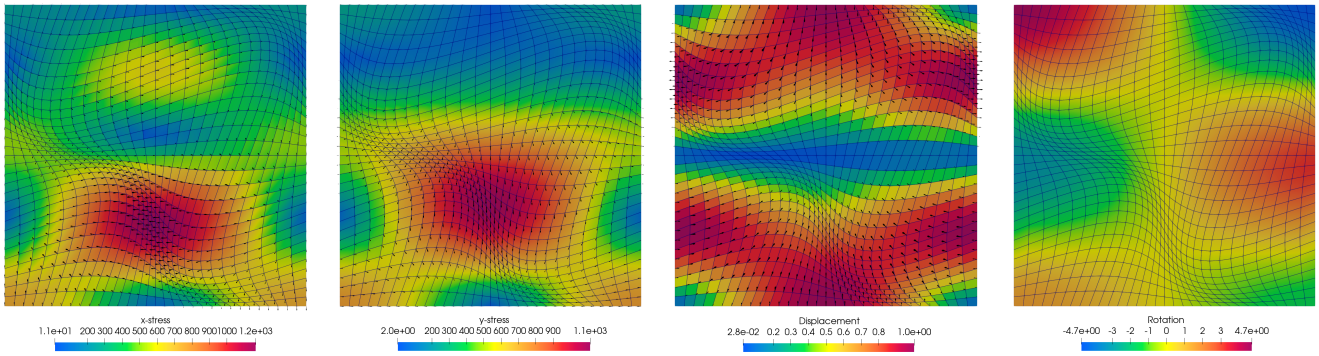

(a) x-stress (b) y-stress (c) Displacement (d) Rotation

Figure 5: Computed solution on a smooth quadrilateral mesh via the MSMFE-1 method, $h = 1/32$.

Table 1: MSMFE-0 method - Convergence on square grids

	$\|\sigma - \sigma_h\|$		$\|\mathrm{div}(\sigma - \sigma_h)\|$		$\|u - u_h\|$		$\|Q_h^u u - u_h\|$		$\|\gamma - \gamma_h\|$	
h	Error	Rate	Error	Rate	Error	Rate	Error	Rate	Error	Rate
1/2	7.684E − 01	–	9.248E − 01	–	7.197E − 01	–	4.984E − 01	–	9.586E − 01	–
1/4	3.786E − 01	1.02	5.455E − 01	0.76	4.574E − 01	0.65	1.208E − 01	2.04	5.059E − 01	0.92
1/8	1.687E − 01	1.17	2.866E − 01	0.93	2.338E − 01	0.97	3.245E − 02	1.90	2.611E − 01	0.95
1/16	8.031E − 02	1.07	1.456E − 01	0.98	1.172E − 01	1.00	8.363E − 03	1.96	1.313E − 01	0.99
1/32	3.959E − 02	1.02	7.326E − 02	0.99	5.861E − 02	1.00	2.108E − 03	1.99	6.570E − 02	1.00
1/64	1.972E − 02	1.01	3.671E − 02	1.00	2.931E − 02	1.00	5.282E − 04	2.00	3.286E − 02	1.00

Table 2: MSMFE-1 method - Convergence on square grids

	$\|\sigma - \sigma_h\|$		$\|\mathrm{div}(\sigma - \sigma_h)\|$		$\|u - u_h\|$		$\|Q_h^u u - u_h\|$		$\|\gamma - \gamma_h\|$	
h	Error	Rate	Error	Rate	Error	Rate	Error	Rate	Error	Rate
1/2	7.614E − 01	–	9.248E − 01	–	7.199E − 01	–	4.758E − 01	–	8.171E − 01	–
1/4	3.742E − 01	1.02	5.455E − 01	0.76	4.561E − 01	0.66	1.057E − 01	2.17	3.909E − 01	1.06
1/8	1.664E − 01	1.17	2.866E − 01	0.93	2.334E − 01	0.97	2.775E − 02	1.93	1.149E − 01	1.77
1/16	7.911E − 02	1.07	1.456E − 01	0.98	1.171E − 01	0.99	7.254E − 03	1.94	3.043E − 02	1.92
1/32	3.897E − 02	1.02	7.326E − 02	0.99	5.860E − 02	1.00	1.841E − 03	1.98	7.753E − 03	1.97
1/64	1.941E − 02	1.01	3.671E − 02	1.00	2.931E − 02	1.00	4.623E − 04	1.99	1.949E − 03	1.99

Table 3: MSMFE-0 method - Convergence on h^2-parallelogram grids

	$\|\sigma-\sigma_h\|$		$\|\mathrm{div}(\sigma-\sigma_h)\|$		$\|u-u_h\|$		$\|Q_h^u u-u_h\|$		$\|\gamma-\gamma_h\|$	
h	Error	Rate	Error	Rate	Error	Rate	Error	Rate	Error	Rate
1/3	5.878E − 01	–	7.179E − 01	–	5.431E − 01	–	2.672E − 01	–	1.026E + 00	–
1/6	2.281E − 01	1.37	3.812E − 01	0.91	3.057E − 01	0.83	7.133E − 02	1.91	4.101E − 01	1.32
1/12	1.021E − 01	1.16	1.943E − 01	0.97	1.567E − 01	0.96	1.585E − 02	2.17	2.056E − 01	1.00
1/24	4.979E − 02	1.04	9.770E − 02	0.99	7.877E − 02	0.99	3.948E − 03	2.01	1.024E − 01	1.01
1/48	2.481E − 02	1.00	4.894E − 02	1.00	3.943E − 02	1.00	9.913E − 04	1.99	5.111E − 02	1.00
1/96	1.241E − 02	1.00	2.449E − 02	1.00	1.972E − 02	1.00	2.486E − 04	2.00	2.554E − 02	1.00

Table 4: MSMFE-1 method - Convergence on h^2-parallelogram grids

	$\|\sigma-\sigma_h\|$		$\|\mathrm{div}(\sigma-\sigma_h)\|$		$\|u-u_h\|$		$\|Q_h^u u-u_h\|$		$\|\gamma-\gamma_h\|$	
h	Error	Rate	Error	Rate	Error	Rate	Error	Rate	Error	Rate
1/3	5.624E − 01	–	7.179E − 01	–	5.179E − 01	–	2.347E − 01	–	7.142E − 01	–
1/6	2.490E − 01	1.18	3.812E − 01	0.91	3.070E − 01	0.75	9.135E − 02	1.36	3.180E − 01	1.17
1/12	1.147E − 01	1.12	1.943E − 01	0.97	1.569E − 01	0.97	2.285E − 02	2.00	1.076E − 01	1.56
1/24	5.666E − 02	1.02	9.770E − 02	0.99	7.881E − 02	0.99	5.966E − 03	1.94	3.584E − 02	1.59
1/48	2.833E − 02	1.00	4.894E − 02	1.00	3.944E − 02	1.00	1.525E − 03	1.97	1.118E − 02	1.59
1/96	1.418E − 02	1.00	2.449E − 02	1.00	1.972E − 02	1.00	3.845E − 04	1.99	3.984E − 03	1.58

Table 5: MSMFE-0 method - Convergence on smooth quadrilateral grids

	$\|\sigma-\sigma_h\|$		$\|\mathrm{div}(\sigma-\sigma_h)\|$		$\|u-u_h\|$		$\|Q_h^u u-u_h\|$		$\|\gamma-\gamma_h\|$	
h	Error	Rate	Error	Rate	Error	Rate	Error	Rate	Error	Rate
1/2	7.684E − 01	–	9.248E − 01	–	7.197E − 01	–	4.984E − 01	–	9.586E − 01	–
1/4	4.340E − 01	0.82	6.224E − 01	0.57	4.699E − 01	0.61	1.429E − 01	1.80	6.306E − 01	0.60
1/8	2.103E − 01	1.05	3.460E − 01	0.85	2.656E − 01	0.82	4.904E − 02	1.54	3.287E − 01	0.94
1/16	9.915E − 02	1.08	1.784E − 01	0.96	1.357E − 01	0.97	1.400E − 02	1.81	1.579E − 01	1.06
1/32	4.862E − 02	1.03	9.001E − 02	0.99	6.816E − 02	0.99	3.650E − 03	1.94	7.864E − 02	1.01
1/64	2.419E − 02	1.01	4.513E − 02	1.00	3.412E − 02	1.00	9.229E − 04	1.98	3.929E − 02	1.00

Table 6: MSMFE-1 method - Convergence on smooth quadrilateral grids

	$\|\sigma-\sigma_h\|$		$\|\mathrm{div}(\sigma-\sigma_h)\|$		$\|u-u_h\|$		$\|Q_h^u u-u_h\|$		$\|\gamma-\gamma_h\|$	
h	Error	Rate	Error	Rate	Error	Rate	Error	Rate	Error	Rate
1/2	7.614E − 01	–	9.248E − 01	–	7.199E − 01	–	4.758E − 01	–	8.171E − 01	–
1/4	4.173E − 01	0.87	6.224E − 01	0.57	4.704E − 01	0.61	1.317E − 01	1.85	4.424E − 01	0.88
1/8	2.062E − 01	1.02	3.460E − 01	0.85	2.662E − 01	0.82	5.084E − 02	1.37	1.994E − 01	1.15
1/16	1.006E − 01	1.04	1.784E − 01	0.96	1.360E − 01	0.97	1.723E − 02	1.56	7.888E − 02	1.34
1/32	4.986E − 02	1.01	9.001E − 02	0.99	6.822E − 02	0.99	4.940E − 03	1.80	2.655E − 02	1.57
1/64	2.487E − 02	1.00	4.513E − 02	1.00	3.413E − 02	1.00	1.293E − 03	1.93	8.560E − 03	1.63

The fourth test employs sequences of quadrilateral grids derived from square grids. Here, at each refinement level, the vertices of the grid are randomly displaced within a sphere of radius $\mathcal{O}(h^\alpha)$, where $\alpha = 1, 1.5, \text{or } 2$. We first present in Tables 7–9 the convergence results on these grids for the symmetric MSMFE-1 method [6]. As expected, convergence is not achieved for all variables on grids perturbed randomly at levels of $\mathcal{O}(h)$ and $\mathcal{O}(h^{1.5})$. In Tables 10–15 we present the convergence results on these grids for the non-symmetric MSMFE-0 and MSMFE-1 methods developed here. Additionally, Figures 6–8 display the computed solutions on these meshes for the MSMFE-1 method. We observe that the solutions are similar despite the different types of grids. The highly distorted elements do not affect the quality of the solution. Moreover the non-symmetric methods achieve at least $\mathcal{O}(h)$ convergence for all variables

in the L^2-norm, verifying the theoretical convergence rates established in Theorem 6.1. As expected, the convergence for the divergence of the stress deteriorates as the grid distortion increases, due to the loss of approximation for $\|\operatorname{div}(\sigma - \Pi\sigma)\|$. This test clearly illustrates the advantage of the MSMFE methods developed in this paper compared to the symmetric methods developed in [6].

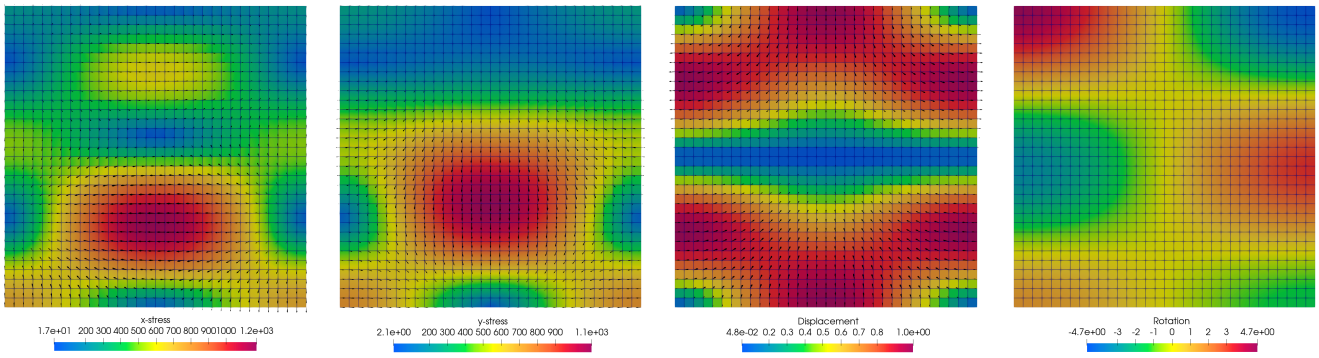

(a) x-stress (b) y-stress (c) Displacement (d) Rotation

Figure 6: Computed solution on a $\mathcal{O}(h^2)$ randomly perturbed mesh via the MSMFE-1 method, $h = 1/32$.

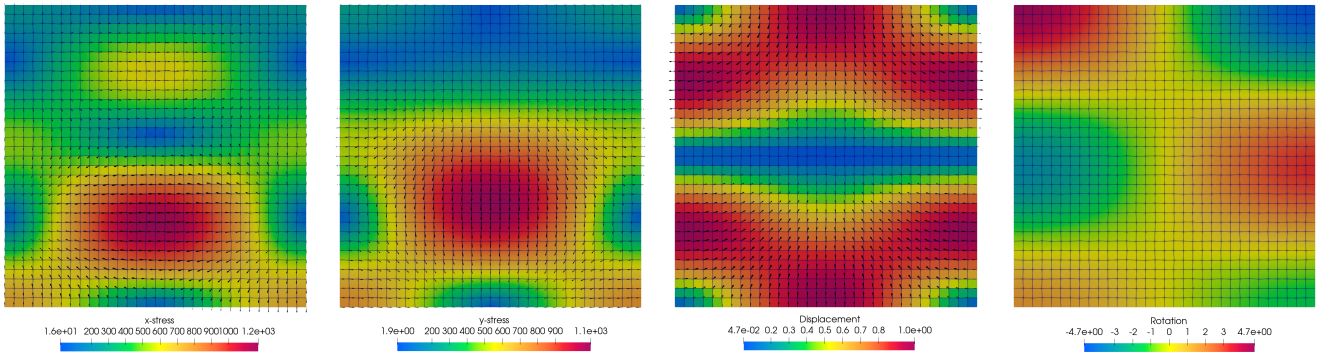

(a) x-stress (b) y-stress (c) Displacement (d) Rotation

Figure 7: Computed solution on a $\mathcal{O}(h^{1.5})$ randomly perturbed mesh via the MSMFE-1 method, $h = 1/32$.

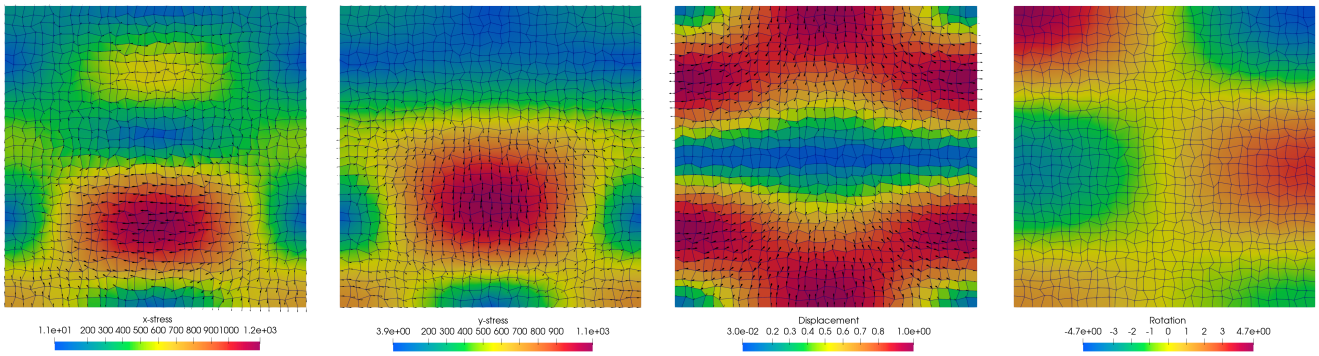

(a) x-stress (b) y-stress (c) Displacement (d) Rotation

Figure 8: Computed solution on a $\mathcal{O}(h)$ randomly perturbed mesh via the MSMFE-1 method, $h = 1/32$.

Table 7: Symmetric MSMFE-1 method - Convergence on $O(h^2)$ randomly perturbed grids

	$\|\sigma-\sigma_h\|$		$\|\mathrm{div}(\sigma-\sigma_h)\|$		$\|u-u_h\|$		$\|Q_h^u u-u_h\|$		$\|\gamma-\gamma_h\|$	
h	Error	Rate	Error	Rate	Error	Rate	Error	Rate	Error	Rate
1/4	3.747E − 01	–	5.456E − 01	–	4.566E − 01	–	1.056E − 01	–	3.902E − 01	–
1/8	1.664E − 01	1.17	2.866E − 01	0.93	2.333E − 01	0.97	2.782E − 02	1.92	1.153E − 01	1.76
1/16	7.912E − 02	1.07	1.456E − 01	0.98	1.171E − 01	0.99	7.255E − 03	1.94	3.044E − 02	1.92
1/32	3.897E − 02	1.02	7.327E − 02	0.99	5.860E − 02	1.00	1.842E − 03	1.98	7.770E − 03	1.97
1/64	1.941E − 02	1.01	3.671E − 02	1.00	2.931E − 02	1.00	4.624E − 04	1.99	1.964E − 03	1.98
1/128	9.696E − 03	1.00	1.837E − 02	1.00	1.465E − 02	1.00	1.157E − 04	2.00	5.025E − 04	1.97

Table 8: Symmetric MSMFE-1 method - Convergence on $O(h^{1.5})$ randomly perturbed grids

	$\|\sigma-\sigma_h\|$		$\|\mathrm{div}(\sigma-\sigma_h)\|$		$\|u-u_h\|$		$\|Q_h^u u-u_h\|$		$\|\gamma-\gamma_h\|$	
h	Error	Rate	Error	Rate	Error	Rate	Error	Rate	Error	Rate
1/4	3.782E − 01	–	5.478E − 01	–	4.591E − 01	–	1.072E − 01	–	3.886E − 01	–
1/8	1.674E − 01	1.18	2.876E − 01	0.93	2.334E − 01	0.98	2.851E − 02	1.91	1.179E − 01	1.72
1/16	7.973E − 02	1.07	1.468E − 01	0.97	1.173E − 01	0.99	7.360E − 03	1.95	3.163E − 02	1.90
1/32	3.950E − 02	1.01	7.435E − 02	0.98	5.863E − 02	1.00	1.889E − 03	1.96	9.803E − 03	1.69
1/64	1.992E − 02	0.99	3.772E − 02	0.98	2.931E − 02	1.00	4.848E − 04	1.96	4.451E − 03	1.14
1/128	1.020E − 02	0.97	1.939E − 02	0.96	1.466E − 02	1.00	1.269E − 04	1.93	2.880E − 03	0.63

Table 9: Symmetric MSMFE-1 method - Convergence on $O(h)$ randomly perturbed grids

	$\|\sigma-\sigma_h\|$		$\|\mathrm{div}(\sigma-\sigma_h)\|$		$\|u-u_h\|$		$\|Q_h^u u-u_h\|$		$\|\gamma-\gamma_h\|$	
h	Error	Rate	Error	Rate	Error	Rate	Error	Rate	Error	Rate
1/4	4.186E − 01	–	5.894E − 01	–	4.856E − 01	–	1.416E − 01	–	3.968E − 01	–
1/8	1.986E − 01	1.08	3.375E − 01	0.80	2.443E − 01	0.99	4.482E − 02	1.66	1.625E − 01	1.29
1/16	1.173E − 01	0.76	2.239E − 01	0.59	1.254E − 01	0.96	1.557E − 02	1.53	8.360E − 02	0.96
1/32	8.929E − 02	0.39	1.835E − 01	0.29	6.285E − 02	1.00	8.819E − 03	0.82	7.584E − 02	0.14
1/64	8.120E − 02	0.14	1.702E − 01	0.11	3.205E − 02	0.97	7.132E − 03	0.31	7.151E − 02	0.08
1/128	7.915E − 02	0.04	1.660E − 01	0.04	1.696E − 02	0.92	6.582E − 03	0.12	7.193E − 02	−0.01

Table 10: MSMFE-0 method - Convergence on $O(h^2)$ randomly perturbed grids

	$\|\sigma-\sigma_h\|$		$\|\mathrm{div}(\sigma-\sigma_h)\|$		$\|u-u_h\|$		$\|Q_h^u u-u_h\|$		$\|\gamma-\gamma_h\|$	
h	Error	Rate	Error	Rate	Error	Rate	Error	Rate	Error	Rate
1/4	3.790E − 01	–	5.456E − 01	–	4.579E − 01	–	1.209E − 01	–	5.057E − 01	–
1/8	1.687E − 01	1.17	2.866E − 01	0.93	2.338E − 01	0.97	3.246E − 02	1.90	2.616E − 01	0.95
1/16	8.031E − 02	1.07	1.456E − 01	0.98	1.172E − 01	1.00	8.367E − 03	1.96	1.323E − 01	0.98
1/32	3.959E − 02	1.02	7.327E − 02	0.99	5.861E − 02	1.00	2.108E − 03	1.99	6.624E − 02	1.00
1/64	1.972E − 02	1.01	3.671E − 02	1.00	2.931E − 02	1.00	5.282E − 04	2.00	3.327E − 02	0.99
1/128	9.852E − 03	1.00	1.837E − 02	1.00	1.465E − 02	1.00	1.321E − 04	2.00	1.687E − 02	0.98
1/256	4.925E − 03	1.00	9.185E − 03	1.00	7.327E − 03	1.00	3.304E − 05	2.00	8.290E − 03	1.02

Table 11: MSMFE-1 method - Convergence on $O(h^2)$ randomly perturbed grids

	$\|\sigma - \sigma_h\|$		$\|\mathrm{div}(\sigma - \sigma_h)\|$		$\|u - u_h\|$		$\|Q_h^u u - u_h\|$		$\|\gamma - \gamma_h\|$	
h	Error	Rate	Error	Rate	Error	Rate	Error	Rate	Error	Rate
1/4	3.744E − 01	–	5.456E − 01	–	4.565E − 01	–	1.051E − 01	–	3.894E − 01	–
1/8	1.664E − 01	1.17	2.866E − 01	0.93	2.334E − 01	0.97	2.775E − 02	1.92	1.150E − 01	1.76
1/16	7.911E − 02	1.07	1.456E − 01	0.98	1.171E − 01	0.99	7.255E − 03	1.94	3.043E − 02	1.92
1/32	3.897E − 02	1.02	7.327E − 02	0.99	5.860E − 02	1.00	1.842E − 03	1.98	7.755E − 03	1.97
1/64	1.941E − 02	1.01	3.671E − 02	1.00	2.931E − 02	1.00	4.623E − 04	1.99	1.949E − 03	1.99
1/128	9.695E − 03	1.00	1.837E − 02	1.00	1.465E − 02	1.00	1.157E − 04	2.00	4.881E − 04	2.00

Table 12: MSMFE-0 method - Convergence on $O(h^{1.5})$ randomly perturbed grids

	$\|\sigma - \sigma_h\|$		$\|\mathrm{div}(\sigma - \sigma_h)\|$		$\|u - u_h\|$		$\|Q_h^u u - u_h\|$		$\|\gamma - \gamma_h\|$	
h	Error	Rate	Error	Rate	Error	Rate	Error	Rate	Error	Rate
1/4	3.817E − 01	–	5.478E − 01	–	4.606E − 01	–	1.224E − 01	–	5.071E − 01	–
1/8	1.695E − 01	1.17	2.876E − 01	0.93	2.339E − 01	0.98	3.284E − 02	1.90	2.726E − 01	0.90
1/16	8.063E − 02	1.07	1.468E − 01	0.97	1.174E − 01	0.99	8.427E − 03	1.96	1.839E − 01	0.57
1/32	3.971E − 02	1.02	7.435E − 02	0.98	5.864E − 02	1.00	2.114E − 03	1.99	1.230E − 01	0.58
1/64	1.976E − 02	1.01	3.772E − 02	0.98	2.931E − 02	1.00	5.291E − 04	2.00	8.284E − 02	0.57
1/128	9.863E − 03	1.00	1.939E − 02	0.96	1.466E − 02	1.00	1.323E − 04	2.00	6.755E − 02	0.29
1/256	4.927E − 03	1.00	1.018E − 02	0.93	7.327E − 03	1.00	3.307E − 05	2.00	2.856E − 02	1.24
1/512	2.463E − 03	1.00	5.541E − 03	0.88	3.664E − 03	1.00	8.262E − 06	2.00	1.212E − 02	1.24

Table 13: MSMFE-1 method - Convergence on $O(h^{1.5})$ randomly perturbed grids

	$\|\sigma - \sigma_h\|$		$\|\mathrm{div}(\sigma - \sigma_h)\|$		$\|u - u_h\|$		$\|Q_h^u u - u_h\|$		$\|\gamma - \gamma_h\|$	
h	Error	Rate	Error	Rate	Error	Rate	Error	Rate	Error	Rate
1/4	3.767E − 01	–	5.478E − 01	–	4.588E − 01	–	1.050E − 01	–	3.860E − 01	–
1/8	1.671E − 01	1.17	2.876E − 01	0.93	2.335E − 01	0.97	2.801E − 02	1.91	1.163E − 01	1.73
1/16	7.927E − 02	1.08	1.468E − 01	0.97	1.173E − 01	0.99	7.307E − 03	1.94	3.090E − 02	1.91
1/32	3.900E − 02	1.02	7.435E − 02	0.98	5.863E − 02	1.00	1.847E − 03	1.98	8.005E − 03	1.95
1/64	1.942E − 02	1.01	3.772E − 02	0.98	2.931E − 02	1.00	4.630E − 04	2.00	2.077E − 03	1.95
1/128	9.697E − 03	1.00	1.939E − 02	0.96	1.466E − 02	1.00	1.158E − 04	2.00	5.488E − 04	1.92

Table 14: MSMFE-0 method - Convergence on $O(h)$ randomly perturbed grids

	$\|\sigma - \sigma_h\|$		$\|\mathrm{div}(\sigma - \sigma_h)\|$		$\|u - u_h\|$		$\|Q_h^u u - u_h\|$		$\|\gamma - \gamma_h\|$	
h	Error	Rate	Error	Rate	Error	Rate	Error	Rate	Error	Rate
1/4	4.185E − 01	–	5.894E − 01	–	4.886E − 01	–	1.587E − 01	–	5.269E − 01	–
1/8	1.948E − 01	1.10	3.375E − 01	0.80	2.462E − 01	0.99	4.786E − 02	1.73	5.651E − 01	−0.10
1/16	1.020E − 01	0.93	2.239E − 01	0.59	1.256E − 01	0.97	1.452E − 02	1.72	6.201E − 01	−0.13
1/32	5.288E − 02	0.95	1.835E − 01	0.29	6.255E − 02	1.01	4.210E − 03	1.79	3.872E − 01	0.68
1/64	2.543E − 02	1.06	1.702E − 01	0.11	3.134E − 02	1.00	9.382E − 04	2.17	1.512E − 01	1.36
1/128	1.262E − 02	1.01	1.660E − 01	0.04	1.567E − 02	1.00	2.226E − 04	2.08	7.277E − 02	1.06

Table 15: MSMFE-1 method - Convergence on $O(h)$ randomly perturbed grids

	$\|\sigma-\sigma_h\|$		$\|\mathrm{div}(\sigma-\sigma_h)\|$		$\|u-u_h\|$		$\|Q_h^u u-u_h\|$		$\|\gamma-\gamma_h\|$	
h	Error	Rate	Error	Rate	Error	Rate	Error	Rate	Error	Rate
1/4	4.135E − 01	–	5.894E − 01	–	4.853E − 01	–	3.393E − 01	–	4.008E − 01	–
1/8	1.854E − 01	1.16	3.375E − 01	0.80	2.453E − 01	0.98	3.914E − 02	1.83	1.493E − 01	1.43
1/16	8.892E − 02	1.06	2.239E − 01	0.59	1.252E − 01	0.97	1.031E − 02	1.92	5.717E − 02	1.38
1/32	4.350E − 02	1.03	1.835E − 01	0.29	6.245E − 02	1.00	2.622E − 03	1.98	2.554E − 02	1.16
1/64	2.175E − 02	1.00	1.702E − 01	0.11	3.133E − 02	1.00	6.483E − 04	2.02	1.265E − 02	1.01
1/128	1.085E − 02	1.00	1.660E − 01	0.04	1.567E − 02	1.00	1.606E − 04	2.01	6.157E − 03	1.04

8 Conclusions

In this work we presented two MFE methods for linear elasticity with weak stress symmetry on distorted quadrilateral grids, which reduce to positive definite cell-centered algebraic systems. These methods utilize the $\mathcal{BDM}_1$ space for the stress and combine a special non-symmetric vertex quadrature rule in the constitutive equation with a symmetric vertex quadrature rule in the equation enforcing weakly the stress symmetry. The MSMFE-0 method with piecewise constant rotations reduces to a cell-centered scheme for the displacements and rotations, while the MSMFE-1 method with continuous bilinear rotations reduces to a cell-centered scheme for the displacements only.

To analyze the stability and convergence of the methods we establish a bound between the stress-rotation bilinear forms with non-symmetric and symmetric quadrature rules. We demonstrate that the resulting algebraic system for each method is positive definite and prove first-order convergence for all variables in the L^2-norm. The theory is illustrated by numerical experiments, which verify the good performance of both the MSMFE-0 and MSMFE-1 methods on highly distorted quadrilateral grids. A possible topic for future investigation is developing MSMFE methods on hexahedral meshes, building on the MSMFE method on cuboid grids developed in [39].

A Appendix A

In this section we establish Assumption 3.1 on rectangular meshes. The following theorem, proved in [5], provides sufficient conditions for a triple $\mathbb{X}_h \times V_h \times \mathbb{W}_h$ to satisfy (3.5) on any type of finite element partition of Ω.

Theorem A.1. [5, Theorem 4.2] *Suppose that $S_h \subset H(\mathrm{div};\Omega)$ and $U_h \subset L^2(\Omega)$ satisfy, for $c_1 > 0$ independent of h,*

$$\inf_{0\neq r\in U_h} \sup_{0\neq z\in S_h} \frac{(\mathrm{div}\, z, r)}{\|z\|_{\mathrm{div}}\|r\|} \geq c_1, \tag{A.1}$$

that $Q_h \subset H^1(\Omega,\mathbb{R}^2)$ and $W_h \subset L^2(\Omega)$ are such that $(w,w)_{\tilde{Q}}^{1/2}$ is a norm in W_h equivalent to $\|w\|$ and, for $c_2 > 0$ independent of h,

$$\inf_{0\neq w\in W_h} \sup_{0\neq q\in Q_h} \frac{(\mathrm{div}\, q, w)_{\tilde{Q}}}{\|q\|_1\|w\|} \geq c_2, \tag{A.2}$$

and that

$$\mathrm{curl}\, Q_h \subset S_h \times S_h. \tag{A.3}$$

Then, $\mathbb{X}_h = S_h\times S_h \subset H(\mathrm{div};\Omega,\mathbb{M})$, $V_h = U_h\times U_h \subset L^2(\Omega,\mathbb{R}^2)$ and $\mathbb{W}_h = \left\{\xi : \xi = \begin{pmatrix} 0 & w \\ -w & 0 \end{pmatrix},\ w \in W_h\right\} \subset L^2(\Omega,\mathbb{N})$ satisfy (3.5).

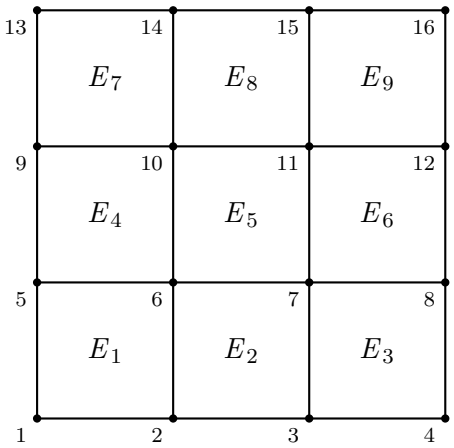

Figure 9: A 3×3 rectangular macroelement.

Condition (A.1) states that $S_h \times U_h$ is a stable Darcy pair. Condition (A.2) states that $Q_h \times W_h$ is a stable Stokes pair with quadrature.

We will apply Theorem A.1 for the spaces $\mathbb{X}_h \times V_h \times \mathbb{W}_h^0$ employed in the MSMFE-0 method. According the definition of the spaces in (2.9) and (2.12), we define

$$\begin{aligned} S_h &= \{z \in H(\mathrm{div};\Omega) : z|_E \overset{\mathcal{P}}{\leftrightarrow} \hat{z} \in \mathcal{BDM}_1(\hat{E}), z \cdot n = 0 \text{ on } \Gamma_N\}, \\ U_h &= \{r \in L^2(\Omega) : r|_E \leftrightarrow \hat{r} \in Q_0(\hat{E})\}, \\ W_h &= \{w \in L^2(\Omega) : w|_E \leftrightarrow \hat{w} \in Q_0(\hat{E})\}. \end{aligned}$$

The boundary condition in S_h is needed to guarantee the essential boundary condition in $\mathbb{X}_h$ on Γ_N. Also, due to Lemma 2.1, W_h satisfies the norm equivalence $(w,w)_{\tilde{Q}}^{1/2} \sim \|w\|$. Next, following the construction in [11], we take $SS_2(\hat{E})$ to be the reduced (serendipity) bi-quadratic space [20],

$$\mathcal{SS}_2(\hat{E}) = P_2(\hat{E}) + \mathrm{span}\{\hat{x}^2\hat{y}, \hat{x}\hat{y}^2\},$$

and define the space Q_h as

$$Q_h = \{q \in H^1(\Omega, \mathbb{R}^2) : q_i|_E \leftrightarrow \hat{q}_i \in SS_2(\hat{E}), \quad i = 1,2, \quad \forall E \in \mathcal{T}_h, \quad q = 0 \text{ on } \Gamma_N\}.$$

Lemma A.1. *Conditions* (A.1) *and* (A.3) *hold for the spaces S_h, U_h, W_h, and Q_h defined above.*

Proof. Since $\mathcal{BDM}_1 \times Q_0$ is known to be a stable Darcy pair [18], condition (A.1) holds. Next, it can be verified that $\mathrm{curl}\,\mathcal{SS}_2(\hat{E}) \subset \mathcal{BDM}_1(\hat{E})$. Since for $q \in Q_h$ we have $q = 0$ on Γ_N, it follows that $(\mathrm{curl}\, q)\, n = 0$ on Γ_N, see [5, Lemma 4.2]. Therefore (2.11) implies that $\mathrm{curl}\, Q_h \subset S_h \times S_h$, i.e. (A.3) holds. □

It remains to show that (A.2) holds. We use the macroelement approach from [34]. Let M be a 3×3 rectangular macroelement as depicted in Figure 9, and assume that $\mathcal{T}_h$ can be agglomerated into a conforming mesh of macroelements M. For a given macroelement M, we consider the span of basis functions associated with the four interior vertex degrees of freedom of $Q_h(M)$, denoted by $Q_h^v(M)$. Define

$$N_M = \{w \in W_h(E) : (\mathrm{div}\, q, w)_{\tilde{Q},M} = 0, \quad \forall q \in Q_h^v(M)\}.$$

Lemma A.2. *N_M is a two-dimensional space with a checkerboard pattern.*

Proof. Let the basis functions for $Q_h^v(M)$ be denoted by q_i^α, where $\alpha = x, y$ and $i = 6, 7, 10, 11$, as shown in Figure 9. For $w \in W_h$, let w_i, $i = 1, \ldots, 9$, be the values of w on E_i. A direct calculation yields

$$(q_6^x, w)_{\tilde{Q},M} = 0.5\left[(y_5 - y_2)w_1 + (y_2 - y_7)w_2 + (y_7 - y_{10})w_5 + (y_{10} - y_5)w_4\right],$$
$$(q_6^y, w)_{\tilde{Q},M} = 0.5\left[(x_2 - x_5)w_1 + (x_7 - x_2)w_2 + (x_{10} - x_7)w_5 + (x_5 - x_{10})w_4\right].$$

From these equations, we obtain the conditions:

$$w_1 - w_2 - w_5 + w_4 = 0,$$
$$w_1 + w_2 - w_5 - w_4 = 0.$$

Solving these equations, we find that $w_1 = w_5$ and $w_2 = w_4$.

By performing similar calculations for the remaining basis functions q_i^α, $i = 7, 10, 11$, and combining the results, we obtain:

$$w_1 = w_3 = w_5 = w_7 = w_9, \quad \text{and} \quad w_2 = w_4 = w_6 = w_8.$$

This confirms that N_M is two-dimensional with a checkerboard pattern, completing the proof. □

Let the projection operator $\mathbb{P}_h$ be defined as $\mathbb{P}_h|_M = \mathbb{P}_h^M$ for all macroelements M, where $\mathbb{P}_h^M$ denote the L^2-projection onto N_M.

Lemma A.3. [5, Lemma 4.7] *There exists a constant $C_1 > 0$ such that for every $w \in W_h$, there exists $q \in Q_h$ satisfying*

$$(\operatorname{div} q, w)_{\tilde{Q}} \geq C_1 \|w - \mathbb{P}_h w\|^2, \quad \textit{and} \quad \|q\|_1 \leq \|w - \mathbb{P}_h w\|.$$

Lemma A.4. *There exists a constant $C_2 > 0$ such that for every $w \in W_h$, there exists $q \in Q_h$ satisfying*

$$(\operatorname{div} q, \mathbb{P}_h w)_{\tilde{Q}} = \|\mathbb{P}_h w\|^2, \quad \textit{and} \quad \|q\|_1 \leq C_2 \|\mathbb{P}_h w\|.$$

Proof. We first construct an interpolant $I_h : H^1(\Omega, \mathbb{R}^2) \to \tilde{Q}_h$ such that

$$(\operatorname{div}(z - I_h z), \mathbb{P}_h w) = 0, \quad \forall w \in W_h, \quad \text{and} \quad \|I_h z\|_1 \leq C\|z\|_1, \tag{A.4}$$

where $\tilde{Q}_h$ is the subspace of Q_h consisting of element-wise mapped bilinear vector functions. We construct I_h on the macroelement M given in Figure 9. In order to satisfy the first property in (A.4), we use that

$$(\operatorname{div}(z - I_h z), \mathbb{P}_h w)_M = \sum_E \int_{\partial E} (I_h z - z) \cdot n \, \mathbb{P}_h w \, ds. \tag{A.5}$$

Considering the vertices and edges in Figure 9, we define I_h as follows:

- $I_h z = z$ at the vertices $\mathbf{r}_1, \mathbf{r}_4, \mathbf{r}_{13}, \mathbf{r}_{16}$.
- On the boundary edge $e_{4,16}$, for the four conditions associated with the vertices $\mathbf{r}_8$ and $\mathbf{r}_{12}$,

  $$\int_{e_{4,8} \cup e_{12,16}} ((I_h z)_1 - z_1)\, ds = 0, \quad \int_{e_{8,12}} ((I_h z)_1 - z_1)\, ds = 0, \quad (I_h z)_2 = z_2 \text{ at } \mathbf{r}_8, \mathbf{r}_{12}.$$

  Similar definitions for the remaining boundary edges.
- For the two conditions associated with vertex $\mathbf{r}_{10}$,

  $$\int_{e_{2,6} \cup e_{10,14}} ((I_h z)_1 - z_1)\, ds = 0, \quad \int_{e_{9,10} \cup e_{11,12}} ((I_h z)_2 - z_2)\, ds = 0.$$

- For the two conditions associated with vertex $\mathbf{r}_7$,

$$\int_{e_{3,7}\cup e_{11,15}} ((I_h z)_1 - z_1)\, ds = 0, \quad \int_{e_{5,6}\cup e_{7,8}} ((I_h z)_2 - z_2)\, ds = 0.$$

- For the two conditions associated with vertex $\mathbf{r}_6$,

$$\int_{e_{6,10}} ((I_h z)_1 - z_1)\, ds = 0, \quad \int_{e_{6,7}} ((I_h z)_2 - z_2)\, ds = 0.$$

- For the two conditions associated with vertex $\mathbf{r}_{11}$,

$$\int_{e_{7,11}} ((I_h z)_1 - z_1)\, ds = 0, \quad \int_{e_{10,11}} ((I_h z)_2 - z_2)\, ds = 0.$$

It is easy to see that this construction defines $I_h z|_M \in \tilde{Q}_h|_M$ uniquely. In addition, the global construction is continuous, i.e. $I_h z \in \tilde{Q}_h$. Using (A.5), it is clear that the construction satisfies the first property in (A.4). The stability bound in (A.4) follows from a scaling argument.

Now, let $w \in W_h$ be arbitrary. There exists $z \in H^1(\Omega, \mathbb{R}^2)$ such that [24, sect.III.3,Exercise 3.4],

$$\operatorname{div} z = \mathbb{P}_h w \quad \text{and} \quad \|z\|_1 \leq C\|\mathbb{P}_h w\|. \tag{A.6}$$

Taking $q = I_h z$ and using (A.4) and (A.6) gives

$$(\operatorname{div} q, \mathbb{P}_h w) = \|\mathbb{P}_h w\|^2, \text{ and } \|q\|_1 \leq C\|\mathbb{P}_h w\|. \tag{A.7}$$

Finally, since q is bilinear, $(\operatorname{div} q, \mathbb{P}_h w) = (\operatorname{div} q, \mathbb{P}_h w)_{\tilde{Q}}$. This, together with (A.7), completes the proof. □

Lemma A.5. *There exist constants $C_3 > 0$ and $C_4 > 0$ such that for every $w \in W_h$, there exists $q \in Q_h$ satisfying*

$$(\operatorname{div} q, w)_{\tilde{Q}} \geq C_3\|w\|^2, \quad \textit{and} \quad \|q\|_1 \leq C_4\|w\|.$$

Proof. Using Lemma A.3 and Lemma A.4, the assertion of the lemma follows from the argument in the proof of Theorem 4.5 in [5]. □

Lemma A.6. *Assumption 3.1 holds on rectangular meshes.*

Proof. The statement of the lemma follows by combining Theorem A.1, Lemma A.1, and Lemma A.5. □

References

[1] I. Aavatsmark. An introduction to multipoint flux approximations for quadrilateral grids. *Comput. Geosci.*, 6(3-4):405–432, 2002. Locally conservative numerical methods for flow in porous media.

[2] I. Aavatsmark, T. Barkve, O. Bøe, and T. Mannseth. Discretization on unstructured grids for inhomogeneous, anisotropic media. II. Discussion and numerical results. *SIAM J. Sci. Comput.*, 19(5):1717–1736, 1998.

[3] I. Aavatsmark, G. T. Eigestad, R. A. Klausen, M. F. Wheeler, and I. Yotov. Convergence of a symmetric MPFA method on quadrilateral grids. *Comput. Geosci.*, 11(4):333–345, 2007.

[4] L. Agelas, C. Guichard, and R. Masson. Convergence of finite volume MPFA O type schemes for heterogeneous anisotropic diffusion problems on general meshes. *Int. J. Finite Vol.*, 7(2):33, 2010.

[5] I. Ambartsumyan, E. Khattatov, J. M. Nordbotten, and I. Yotov. A multipoint stress mixed finite element method for elasticity on simplicial grids. *SIAM J. Numer. Anal.*, 58(1):630–656, 2020.

[6] I. Ambartsumyan, E. Khattatov, J. M. Nordbotten, and I. Yotov. A multipoint stress mixed finite element method for elasticity on quadrilateral grids. *Numer. Methods Partial Differential Equations*, 37(3):1886–1915, 2021.

[7] T. Arbogast, C. N. Dawson, P. T. Keenan, M. F. Wheeler, and I. Yotov. Enhanced cell-centered finite differences for elliptic equations on general geometry. *SIAM J. Sci. Comput.*, 19(2):404–425, 1998.

[8] T. Arbogast, M. F. Wheeler, and I. Yotov. Mixed finite elements for elliptic problems with tensor coefficients as cell-centered finite differences. *SIAM J. Numer. Anal.*, 34(2):828–852, 1997.

[9] D. Arndt, W. Bangerth, D. Davydov, T. Heister, L. Heltai, M. Kronbichler, M. Maier, J.-P. Pelteret, B. Turcksin, and D. Wells. The `deal.II` library, version 8.5. *J. Numer. Math.*, 25(3):137–146, 2017.

[10] D. N. Arnold and G. Awanou. Rectangular mixed finite elements for elasticity. *Math. Models Methods Appl. Sci.*, 15(9):1417–1429, 2005.

[11] D. N. Arnold, G. Awanou, and W. Qiu. Mixed finite elements for elasticity on quadrilateral meshes. *Adv. Comput. Math.*, 41(3):553–572, 2015.

[12] D. N. Arnold, D. Boffi, and R. S. Falk. Quadrilateral $H(\mathrm{div})$ finite elements. *SIAM J. Numer. Anal.*, 42(6):2429–2451, 2005.

[13] D. N. Arnold, F. Brezzi, and J. Douglas, Jr. PEERS: a new mixed finite element for plane elasticity. *Japan J. Appl. Math.*, 1(2):347–367, 1984.

[14] D. N. Arnold, R. S. Falk, and R. Winther. Mixed finite element methods for linear elasticity with weakly imposed symmetry. *Math. Comp.*, 76(260):1699–1723, 2007.

[15] D. N. Arnold and R. Winther. Mixed finite elements for elasticity. *Numer. Math.*, 92(3):401–419, 2002.

[16] G. Awanou. Rectangular mixed elements for elasticity with weakly imposed symmetry condition. *Adv. Comput. Math.*, 38(2):351–367, 2013.

[17] D. Boffi, F. Brezzi, and M. Fortin. Reduced symmetry elements in linear elasticity. *Commun. Pure Appl. Anal.*, 8(1):95–121, 2009.

[18] D. Boffi, F. Brezzi, and M. Fortin. *Mixed finite element methods and applications*, volume 44. Springer, 2013.

[19] F. Brezzi, J. Douglas, Jr., and L. D. Marini. Two families of mixed finite elements for second order elliptic problems. *Numer. Math.*, 47(2):217–235, 1985.

[20] P. G. Ciarlet. *The finite element method for elliptic problems*, volume 40 of *Classics in Applied Mathematics*. Society for Industrial and Applied Mathematics (SIAM), Philadelphia, PA, 2002. Reprint of the 1978 original [North-Holland, Amsterdam; MR0520174 (58 #25001)].

[21] B. Cockburn, J. Gopalakrishnan, and J. Guzmán. A new elasticity element made for enforcing weak stress symmetry. *Math. Comp.*, 79(271):1331–1349, 2010.

[22] M. G. Edwards and C. F. Rogers. Finite volume discretization with imposed flux continuity for the general tensor pressure equation. *Comput. Geosci.*, 2(4):259–290, 1998.

[23] R. E. Ewing, R. D. Lazarov, and P. S. Vassilevski. Local refinement techniques for elliptic problems on cell-centered grids. I. Error analysis. *Math. Comp.*, 56(194):437–461, 1991.

[24] G. P. Galdi. *An introduction to the mathematical theory of the Navier-Stokes equations. Vol. I.* Springer-Verlag, New York, 1994. Linearized steady problems.

[25] J. Gopalakrishnan and J. Guzmán. A second elasticity element using the matrix bubble. *IMA J. Numer. Anal.*, 32(1):352–372, 2012.

[26] R. Ingram, M. F. Wheeler, and I. Yotov. A multipoint flux mixed finite element method on hexahedra. *SIAM J. Numer. Anal.*, 48(4):1281–1312, 2010.

[27] M. Juntunen and J. Lee. A mesh-dependent norm analysis of low-order mixed finite element for elasticity with weakly symmetric stress. *Math. Models Methods Appl. Sci.*, 24(11):2155–2169, 2014.

[28] E. Keilegavlen and J. M. Nordbotten. Finite volume methods for elasticity with weak symmetry. *Int. J. Numer. Meth. Engng.*, 112(8):939–962, 2017.

[29] R. A. Klausen and R. Winther. Robust convergence of multi point flux approximation on rough grids. *Numer. Math.*, 104(3):317–337, 2006.

[30] J. J. Lee. Towards a unified analysis of mixed methods for elasticity with weakly symmetric stress. *Adv. Comput. Math.*, 42(2):361–376, 2016.

[31] K. Lipnikov, M. Shashkov, and I. Yotov. Local flux mimetic finite difference methods. *Numer. Math.*, 112(1):115–152, 2009.

[32] J. M. Nordbotten. Convergence of a cell-centered finite volume discretization for linear elasticity. *SIAM J. Numer. Anal.*, 53(6):2605–2625, 2015.

[33] T. F. Russell and M. F. Wheeler. Finite element and finite difference methods for continuous flows in porous media. In *The mathematics of reservoir simulation*, volume 1, pages 35–106. SIAM, 1983.

[34] R. Stenberg. Analysis of mixed finite elements methods for the Stokes problem: a unified approach. *Math. Comp.*, 42(165):9–23, 1984.

[35] R. Stenberg. A family of mixed finite elements for the elasticity problem. *Numer. Math.*, 53(5):513–538, 1988.

[36] J. Wang and T. Mathew. Mixed finite element methods over quadrilaterals. In *Conference on Advances in Numerical Methods and Applications, IT Dimov, B. Sendov, and P. Vassilevski, eds., World Scientific, River Edge, NJ*, pages 203–214, 1994.

[37] M. Wheeler, G. Xue, and I. Yotov. A multipoint flux mixed finite element method on distorted quadrilaterals and hexahedra. *Numer. Math.*, 121(1):165–204, 2012.

[38] M. F. Wheeler and I. Yotov. A multipoint flux mixed finite element method. *SIAM J. Numer. Anal.*, 44(5):2082–2106, 2006.

[39] I. Yazici and I. Yotov. Multipoint stress mixed finite element methods for elasticity on cuboid grids. arXiv:2502.00163 [math.NA], 2025.